Article

New Acridine Thiourea Gold(I) Anticancer Agents: Targeting the Nucleus and Inhibiting Vasculogenic Mimicry

Sergio A. Pérez, Concepcion de Haro, Consuelo Vicente, Antonio Donaire, Ana Zamora, Juraj Zajac, Hana Kostrhunova, Viktor Brabec, Delia Bautista, and José Ruiz

Just Accepted

1
2
3
4
5
6
7
8
9
10
11
12
13
14
15
16
17
18
19
20
21
22
23
24
25
26
27
28
29
30
31
32
33
34
35
36
37
38
39
40
41
42
43
44
45
46
47
48
49
50
51
52
53
54
55
56
57
58
59
60

New Acridine Thiourea Gold(I) Anticancer Agents: Targeting the Nucleus and Inhibiting Vasculogenic Mimicry

Sergio A. Pérez,[†] Concepción de Haro,[†] Consuelo Vicente,[†] Antonio Donaire,[†] Ana Zamora,[†] Juraj Zajac,[‡,#] Hana Kostrhunova,[‡] Viktor Brabec,[‡] Delia Bautista,[§] and José Ruiz[†]*

[†]Departamento de Química Inorgánica, Facultad de Química, Biomedical Research Institute of Murcia (IMIB-Arrixaca-UMU), Universidad de Murcia, E-30071 Murcia, Spain

[‡]Institute of Biophysics, Academy of Sciences of the Czech Republic, v.v.i. Kralovopolska 135, 612 65 Brno, Czech Republic

[#]Department of Biophysics, Faculty of Science, Palacky University, Slechtitelu 27, 783 71 Olomouc, Czech Republic

[§]SAI., Universidad de Murcia, E-30071-Murcia, Spain

ABSTRACT

Two new 1-acridin-9-yl-3-methylthiourea Au(I) DNA intercalators [Au(ACRTU)$_2$]Cl (**2**) and [Au(ACRTU)(PPh$_3$)]PF$_6$ (**3**) have been prepared. Both complexes were highly active in human ovarian carcinoma cisplatin-sensitive A2780 cell line, exhibiting IC$_{50}$

1

values in the sub-micromolar range. **2** and **3** are also cytotoxic toward different

phenotypes of breast cancer cell lines MDA-MB-231 (triple negative), SK-BR-3

(HER2+, ERα− and ERβ−) and MCF-7 (ER+). Both complexes induce apoptosis

through activation of caspase-3 *in vitro*. While inhibition of some proteins (thiol-

containing enzymes) seems to be the main mechanism of action for cytotoxic gold

complexes, **2** and **3** present a DNA-dependent mechanism of action. They locate in cell

nucleus according to confocal microscopy and transmission electronic microscopy. The

binding to DNA resulted to be via intercalation as shown by spectroscopic methods and

viscometry, exhibiting a dose-dependent response on topoisomerase I mediated DNA

unwinding. In addition, **2** and **3** exhibit potent antiangiogenic effects, and are also able

to inhibit vasculogenic mimicry of highly invasive MDA-MB-231 cells.

1. INTRODUCTION

Cisplatin (CDDP), carboplatin and oxaliplatin have become established drugs in

therapy various solid cancers.[1-4] However, their clinical use has been restricted due to

serious problems such as resistance, nephrotoxicity and neurotoxicity.[5-7] In order to

circumvent these limitations, different research groups have attracted their attention to

complexes of other precious metals as therapeutic agents.[1,2,4,8-14] In this context, gold(I)

and gold(III) compounds have received increasing attention throughout the last decade

as anticancer agents.[15-29]

Auranofin and Et$_3$PAuCl (Figure 1A)[19,22,27] are two interesting complexes that display

their antiproliferative activities specially by interfering with mitochondrial thioredoxin

reductase (TrxR).[30-34] In addition, more Au(I) compounds have been identified to trigger

their antitumor properties through the inhibition of different enzymes. For example, the

cytotoxic triphenylphosphine complex [Au(NHC)(PPh$_3$)]I (Figure 1A) inhibits the

poly(ADP-ribose) polymerase 1,[35] and several gold(I) thiourea-functionalized

2

complexes are tyrosine kinase inhibitors[36] while others, such as [Au(TU)$_2$]Cl (TU = 1,3-bis(4-methoxyphenyl)imidazolidine-2-thione),[37] are thioredoxin reductase inhibitors. On the contrary, it is well known that some Au(III) compounds interact with DNA covalently [38,39] or induce cell death as effective topoisomerase inhibitors.[40]

On the other hand, solid tumors need an adequate nutrients and oxygen supply to allow continued growth and metastasis.[41,42] Thus, inhibition of angiogenesis is a desirable goal,[41,43,44] and combination of angiogenesis inhibitors with chemotherapy would be of great interest.[10,45-47] Several metal complexes have been recently reported as angiogenesis inhibitors[48-58] including Au(I) and Au(III) complexes shown in Figure 1B.
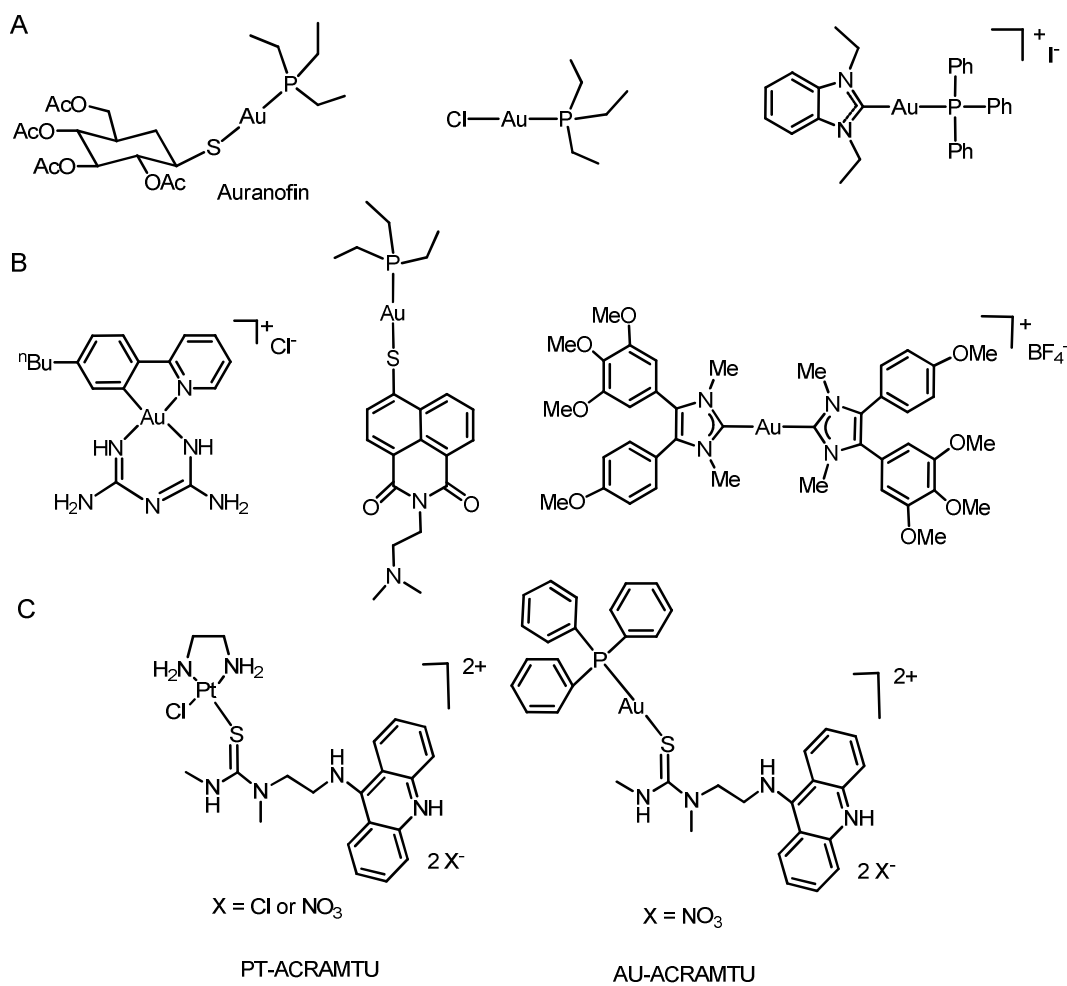
Figure 1. Some antitumor active gold complexes (A) and dual antiangiogenic and antitumor gold complexes (B)[33,55,58] The so-called PT-ACRAMTU and AU-ACRAMTU prepared by Bierbach (*vide infra*) (C).

In addition, vascular mimicry[41,59,60] (VM) enables an additional dissemination way within the tumor,[61-63] and in fact, current anti-vascular therapies targeting endothelial cells are not relevant in VM tumors. Therefore dual action compounds for inhibiting both vasculogenic mimicry and angiogenesis are required to improve the clinical results.[64,65,66]

Prompted by the success of the so-called PT-ACRAMTU (ACRAMTU = 1-[2-(acridin-9-ylamino)ethyl]-1,3-dimethylthiourea), a DNA-targeted platinum-acridine conjugate,[67,68] and the dicationic gold(I) analogue AU-ACRAMTU (Figure 1C) which shows a potent activity against *Mycobacterium tuberculosis*,[69] we have prepared two close-related acridine gold(I) complexes, $[Au(ACRTU)_2]Cl$ and $[Au(ACRTU)(PPh_3)]PF_6$ (ACRTU= 1-acridin-9-yl-methylthiourea), in order to explore their antitumor activity together with their possible anti-angiogenic properties. We have aimed to more thoroughly elucidate their mechanism of action in ovarian and breast cancer cell lines, with a wide variety of *in vitro* and biochemical techniques, including apoptosis studies and intracellular localization studies by confocal microscopy and transmission electron microscopy. In addition, their DNA intercalating characteristics have been studied by spectroscopic methods, viscosity measurements and topoisomerase I inhibition studies. Finally, the angiogenesis inhibiting properties of the new Au(I) compounds in the immortalized humanendothelial cell line EA.hy926 and the vasculogenic mimicry effect in the highly invasive MDA-MB-231 cells have been studied.

4

2. RESULTS AND DISCUSSION

2.1. Synthesis and Characterization of the Au(I) Compounds. *2.1.1. Synthesis of the New Complexes.* The gold complexes **2** and **3** (Chart 1) were prepared from the reaction of the previously reported 1-acridin-9-yl-3-methylthiourea ACRTU ligand[68] (**1**) in the proper molar ratio and solvent with [AuCl(tht)] (tht = tetrahydrothiophene) or [AuClPPh$_3$], respectively. Complexes **2** and **3** were characterized by NMR in DMSO-d$_6$ (Figures S1-S8 in the Supporting Information), IR and UV-vis spectroscopy. The ^{31}P NMR spectrum of **3** shows a unique resonance for coordinated PPh$_3$ ligand (Figure S5). The characteristic optical properties of complexes **2** and **3** were assigned mainly to intraligand (IL) transitions centered on the acridine group (Figure S9). Elemental analyses showed that the purity of the compounds was at least 95%, and their positive-ion ESI-MS displayed the [M]$^+$ peaks in agreement with the calculated isotopic pattern. HPLC chromatogram of **2** shows a single peak at retention time of 11.1 min (Figure S11A) corresponding to complex **2** according to MS TOF spectrum, while the HPLC chromatogram of **3** followed by MS TOF studies indicated that it undergoes partial disproportionation in homoleptic complexes **2** and [Au(PPh$_3$)$_2$]$^+$ (Figure S11B), maybe because the lack of stability for **3** in the column and/or the acidic media used for this experiment.

Chart 1

1

2

3
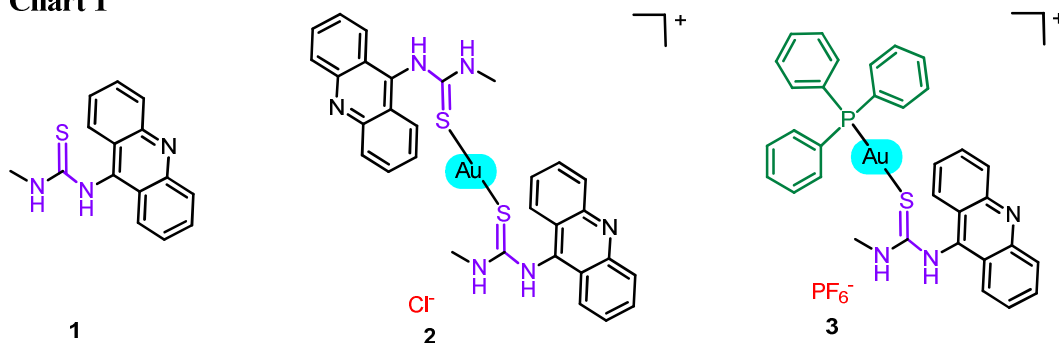
2.1.2. Structure Determination of Complex 3. The crystal structure of **3** has been established by X-ray diffraction (Figure 2). The structure confirms the formation of a 1:1 conjugate with the ligand being connected to an almost linear gold through thiourea sulfur. Intermolecular π-π interactions between acridine ligands are observed and molecules of **3** are stacked to give centrosymmetric pairs (Figure S12). Intermolecular interactions contacts C–H···F–P and N–H···F–P are also observed (Table S3 and Figure S13).
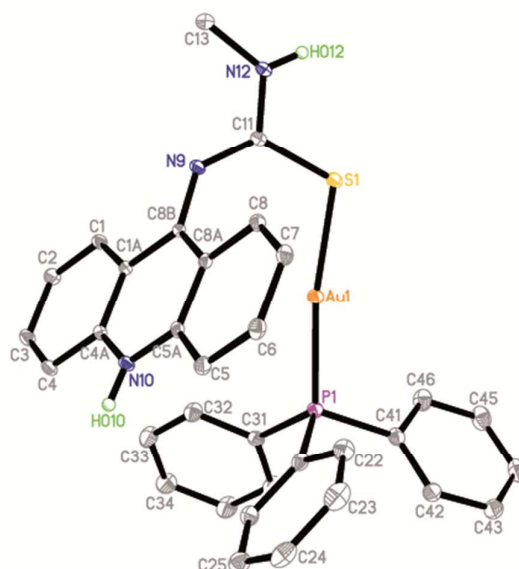
Figure 2. Molecular structure of gold cation with atom numbering schemes for **3** (30% thermal ellipsoids). Selected bond lengths (Å) and angles (deg): Au(1)–P(1) = 2.2639(5), Au(1)–S(1) = 2.3017(5), P(1)–Au(1)–S(1) = 171.027(17).

2.2. Biological Activity. *2.2.1. Cytotoxicity Studies.* The cytotoxicity of **2** and **3** was evaluated (Table 1 and Figures S14 and S15) towards A2780 cells and a panel of human breast cancer cell lines, MDA-MB-231 (triple negative), SK-BR-3 (HER2+, ERα− and ERβ−) and MCF-7 (ER+). The cytotoxicity of CDDP, the free ligand **1** and AuClPPh$_3$ was also determined for comparison purposes.

The results in Table 1 show a distinct antiproliferative activity of the compounds **2** and **3** according to the tested cell lines. Compound **3** resulted to exhibit a higher potency than **2** in all the studied cell lines, being both complexes extremely cytotoxic (submicromolar IC_{50}) toward A2780 cells. This effect, although high, is not so acute for the breast cancer cell lines. Interestingly, both compounds exhibit the higher activity in the negative MDA-MB-231 cell line, becoming approximately 13x more cytotoxic than CDDP. It is to be noted that the ligand **1** is not cytotoxic ($IC_{50} > 50$ μM except for MDA-MB-231) and complex $AuClPPh_3$ shows relatively low IC_{50} values (5.60−14 μM), although always higher than **3**.

Table 1. IC_{50} (μM) for CDDP, $AuClPPh_3$ and Compounds **1**−**3** at 48 h.

Compound	A2780	MDA-MB-231	SK-BR-3	MCF-7	LLC-PK1	EA.hy926
1	> 50	10.94 ± 0.56	> 50	> 50	-	-
2	0.88 ± 0.20	2.75 ± 0.40	3.62 ± 0.14	5.32 ± 0.65	8.56 ± 2.64	3.57 ± 0.16
3	0.40 ± 0.18	2.69 ± 0.87	1.98 ± 0.33	2.35 ± 0.39	2.57 ± 0.38	1.17 ± 0.07
$AuClPPh_3$	14 ±1	10.33 ± 3.81	5.60 ± 0.24	8.68 ± 0.29	-	-
CDDP	2.88 ± 0.09	34.90 ± 7.54	7.79 ± 0.56	12.58 ± 1.88	3.10 ± 0.07	9.86 ± 0.36

Due to the high stability of **2** and **3** in solution, no free ligand was detected by ^{1}H NMR after 24 h incubation in mixtures of DMSO-d_6/D_2O (1:1) (Figure S16) and DMSO-d_6/D_2O (100 mM NaCl) (1:1) (Figure S17), the cytotoxic effect was exclusively attributed to the gold complexes or its metabolites.

2.2.2. Cell-Selectivity of Au(I)-Acridine Complexes 2 and 3 in A2780 and MDA-MB-231. We have found that **2** and **3** were more selective for cancerous cells over healthy cells than CDDP. Table 1 show their IC_{50} values in a kidney healthy cell line, LLC-PK1. Thus, selectivity factors[47] for **2** and **3** (Figure S18) range from 6−9x in A2780 to 10−35x in MDA-MB-231 cells. Likewise, IC_{50} values for **2** and **3** in the EA.hy926 cell

line were also determined (Table 1), showing that their ability to inhibit angiogenesis took place at sub-cytotoxic concentrations (*vide infra*, Section 2.4).[47]

2.2.3. Apoptosis Studies. Apoptotic studies were undertaken in MDA-MB-231 cell line by flow cytometric assay.[47] As it can be seen in Figure 3, **2** and **3** caused an elevated percentage of apoptosis (82 and 98% respectively) in MDA-MB-231 cells. Similar values were found in MCF-7 cells after 24 h of incubation with **2** and **3** (Figure S19). TEM images (Figure 7) supported also apoptosis (*vide infra*).
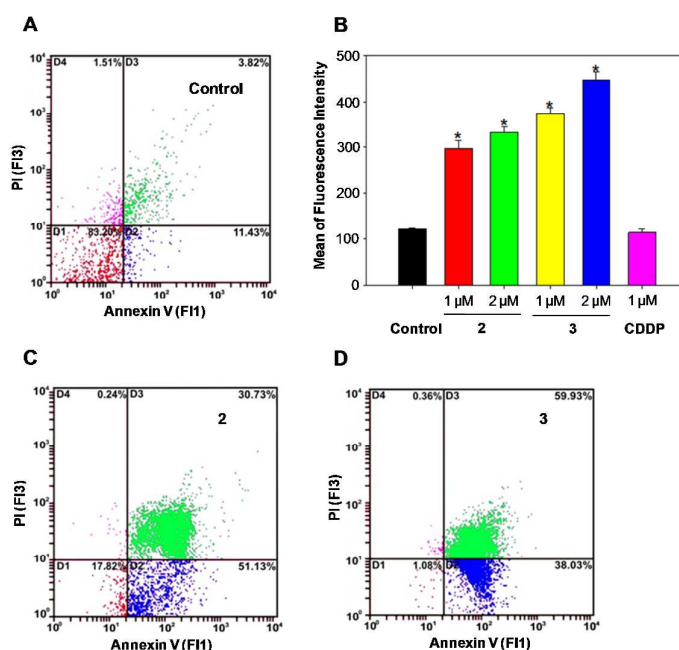
Figure 3. Apoptosis analysis of MDA-MB-231 cells after 24 h for untreated cells (A) and treatment with **2** (C) and **3** (D) using an annexin V/PI assay (at concentrations 2 × IC_{50}). Caspase-3 activation in MDA-MB-231 cells caused by exposure to complexes **2**, **3** and CDDP (B). *$p < 0.05$ was considered to be statistically significant. The results are expressed as mean values ± SD for two independent samples for each compound.

To clarify the mechanism by which the complexes induce apoptosis, the activity of caspase-3, a cysteine protease,[70] was studied using the caspase-3 fluorescence detection

kit (FITC-DEVD-FMK) in MDA-MB-231 (Figure 3B) and MCF-7 (Figure S19B) cell line after 24 h exposure to the complexes **2** and **3** (1 or 2 μM). As shown in Figure 3B, an increase of caspase-3 activity is noted for the compounds with respect to the control and CDDP. Therefore, **2** and **3** induce apoptosis through activation of caspase-3 *in vitro*.

2.2.4. Cell Cycle Arrest. The effect of Au(I) compounds on the cell cycle was examined. MDA-MB-231 cells were exposed to the compounds at concentrations corresponding to their IC_{50} for 24 h at 37 ºC, collected then treated with 70% (vol) EtOH, RNase and dyed with PI and finally, analyzed by flow cytometry. The histograms obtained for **2** and **3** are shown in Figure 4. As can be observed in Figure 4B an increased amount of cells stalled in the G2/M phase ocurred due to the presence of **2** and **3**. Therefore, the G2/M checkpoints impedes the entry into mitosis as result of DNA damaging agents,[71,72] leading the cells to die through apoptosis.
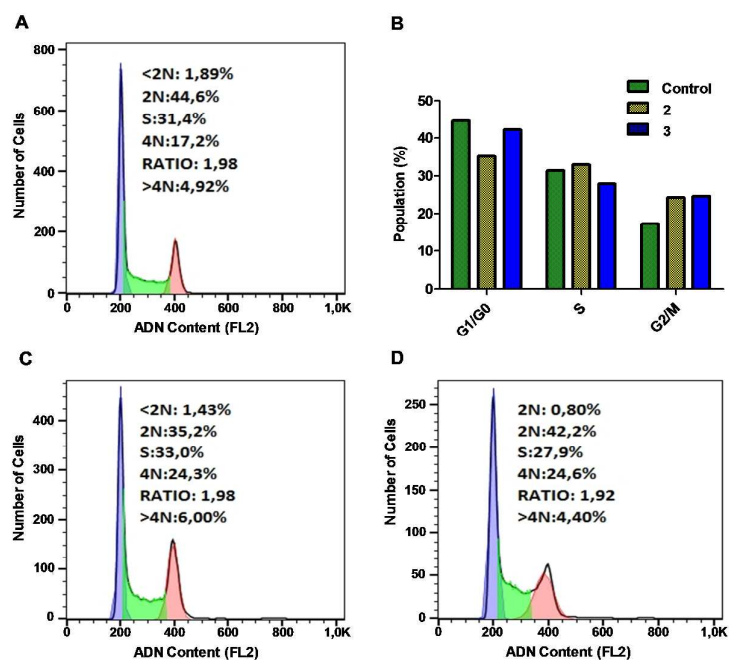
Figure 4. Cell cycle analysis of MDA-MB-231 cells. IP fluorescence intensity (FL2) for negative control (A) and cells exposed to **2** (C) and **3** (D). Effect of **2** and **3** in the studied cell cycle distribution after 24 h incubation (B).

*2.2.5. Cellular Localization of Ligand **1** and Complexes **2** and **3** by Confocal Microscopy.* Intracellular distribution of **1–3** was investigated in MCF-7 cells. Mitochondria and nuclei were stained for 30 min with 100 nM of the far red-fluorescent dye MitoTracker Red and DAPI (binds strongly to A-T rich regions), respectively. After 2 h incubation with **2** (5 μM) and **3** (2 μM), the complexes were excited at a wavelength that does not interfere with the other dyes. The luminescence of **2** and **3** was highly visible in the tumor cells (Figure 5F). It can be observed that the area of the emission of **2** or **3** (Figure 5 E) does not superimpose with MitoTracker Red dye (Figure 5G).

Figure 5. Determination of intracellular localization of **1**-**3** by costaining experiments with DAPI and MitoTracker Red in MCF-7 cells. Phase contrast (A) and (D). Ligand **1** (B) and overlay of phase contrast and **1** (C). Overlay images of DAPI and phase contrast (E). Overlay image of **2** or **3** and phase contrast (F). MitoTracker Red f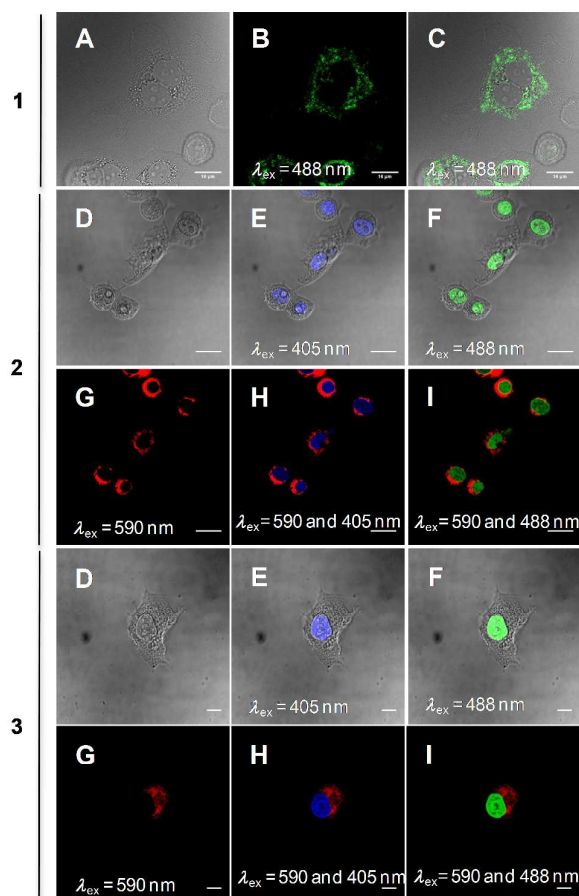luorescence images (G). Dual excitation images of DAPI and MitoTracker Red (H). Dual excitation image of **2** or **3** and MitoTracker Red (I). Scale bar = 30 μm.

In order to avoid possible fluorescence bleed through from DAPI in previous experiment, we have undertaken also confocal microscopic studies of MCF-7 cells treated with **2** or **3** alone (Figure S20). It shows clearly that the complexes accumulate mainly in the nucleus. In addition, as shown in Figures 5B and 5C, ligand **1** is a strong emitter in the cytosol of MCF-7 cells, but surprisingly not in the nucleus in the same experimental conditions used for complexes **2** and **3**. This rather unexpected result could be one of the reasons for the lack of cytotoxicity of **1** in this cancer cell line. Indeed, the non fluorescence signal in the nucleus for ligand **1** may be explained assuming that 2 h was not enough time to accumulate into the nucleus, although another possibility might be a quenching process in this organelle.[73] Notably, the lack of extranuclear emission in Figure 5F indicates that no significant dissociation of acridine ligand in the cytoplasm is observed.

2.2.6. Transmission Electron Microscopy (TEM). This technique can be very useful for the study of cancer cells treated with the gold complexes, as is a third-row transition metal and thus it has a high electron density. None of the conventional staining agents[74] was added, therefore images were as consequence of the added gold compound. Ultrathin sections of MDA-MB-231 and MCF-7 cells treated with **2** and **3** (2 μM) at 37 ºC for 24 h were observed under TEM as shown in Figure 6. A higher contrast, in

particular in the nucleus and nucleolus, is observed for cells treated with **2** (Figures 6B

and 6E) and **3** (Figures 6C and 6F) compared to the control. In addition, more electron

density is observed both in euchromatin and heterochromatin in treated cells with both

complexes in comparison with the control, so the packing of DNA does not affect to the

complexation of DNA-gold complexes. The results are in agreement with the confocal

microscopy and indicate that these compounds mainly interact with nuclear DNA.

Furthermore, it is noteworthy that some cells showed changes related to apoptosis, such

as blebs at the cell surface (Figure 6B) and cytoplasmic vacuolization (Figure 6F).
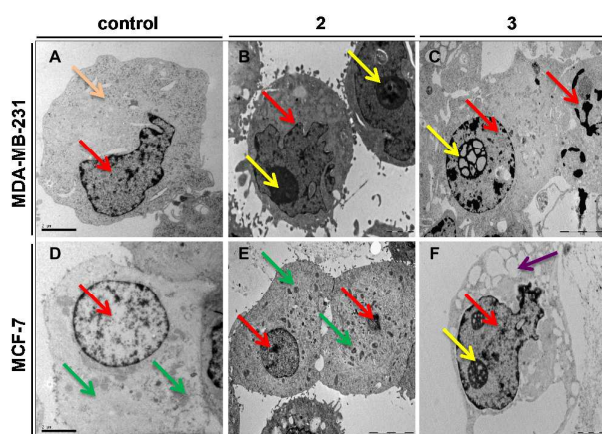
Figure 6. TEM images of untreated MDA-MB-231 cells (A) and treated with **2** (B), **3**

(C). Images of untreated MCF-7 cells (D) or treated with **2** (E), **3** (F). Nucleus (➔),

nucleolus (➔), mitochondria (➔), cytoplasmic vacuolization (➔) and cytoplasm (➔)

can be distinguished. Cells in an early (E) or late (C) stage of apoptosis can be

distinguished.

2.2.7. Cellular Internalization and Accumulation Studies. Internalization studies for

1−3 (5 μM) in A2780 and MCF-7 cells have been undertaken after different incubation

times (2 min, 30 min and 1 h) by flow cytometry. As observed in Figure S21 the free

ligand **1** and the new complexes are able to internalize into cancer cells very easily

12

(even after 2 min). Both A2780 and MCF-7 cells exhibited very low level of autofluorescence (negative controls in Figure S21). The total cellular accumulation of gold complexes and CDDP in A2780 cell line was studied in order to investigate a possible relationship between the cellular uptake and *in vitro* cytotoxicity. Concentrations of metals in cells exposed to complexes (1 μM) for 24 h were measured by ICP-MS.[75] The results are shown in Table 2. A direct relationship between Au accumulation and activity in A2780 cell line is clearly observed in our measurements. Accordingly to log *P* (Table 2) and RP-HPLC studies[10,76] (Figure S11), the most hydrophobic complex **3**, which is 2-fold more cytotoxic than **2** (Table 1), accumulates to the highest extent in A2780 cells. Therefore, there is also a clear relationship between a higher hydrophobicity and an increase in cellular accumulation. As an increase in lipophilicity causes enhanced cellular accumulation, it is probably that passive diffusion plays a major role in the mechanism of cellular accumulation for the compounds.[75]

Table 2. Accumulation of gold compounds and CDDP in A2780 cells treated for 24 h at 1 μM, and log *P* values.

	pmol/10^6 cells[a]	ng/10^6 cells[a]	log P[b]
2	39 ± 2	7.6 ± 0.4	0.57 ± 0.07
3	59 ± 4	12 ± 1	0.79 ± 0.03
CDDP	10 ± 2	1.9 ± 0.4	-2.30 ± 0.04

[a]Total cellular uptake of tested compounds.
[b]Log *P* (octanol/water) values measured at room temperature.[75]
All results are expressed as the mean ± SD from at least three independent experiments.

The results of cellular localization for **2** and **3** by confocal microscopy and transmission electron microscopy (sections 2.2.5. and 2.2.6.) show that both complexes accumulate preferentially in the cell nucleus, where DNA is localized. Thus, it is reasonable to assume that **2** and **3**, after they accumulate in tumor cells, preferentially interact with DNA in the cell nucleus and not with RNA, since most of RNAs are localized in the cytoplasm. Therefore, further studies were focused on understanding interactions of **2** and **3** with DNA in cell-free media.

2.2.8. No Mitochondrial-Disrupting Activity. The possible mitochondrial-destabilizing activity of the compounds was rejected after the study of the intracellular reactive oxygen species (ROS) production and the mitochondrial membrane potential. 2',7'-Dichlorodihydrofluorescein diacetate (DCFH-DA) was used to measure by flow cytometry[77-79] the effect of **2** and **3** on the intracellular production of ROS in MCF-7 and MDA-MB-231 cells (Figure S22). After 24 h incubation of cells with **2** or **3** (1 or 2 µM, a concentration closed to their IC_{50}) and 30 min after the addition of DCFH-DA, the resulting green fluorescence of the oxidation product DCF (2′,7′-dichlorofluorescein) was measured. No increments of ROS production were observed after the exposure of **2** and **3** with respect to the control.

Mitochondria maintain a high negative transmembrane potential at their inner membrane due to generation of ATP through electron transport chain. This unique physical property can be exploited for mitochondrial targeting by using positively charged moieties. For example, Rho-123, a fluorescent lipophilic dye with a delocalized positive charge ($pK_a > 10$) on the xanthenes ring, is highly specific for mitochondria in living cells.[80-82] The small variation in the fluorescence of Rho-123 after the treatment of MCF-7 and MDA-MB-231 cells with the complexes (Figure S23), indicate no changes in the mitochondrial membrane potential. These results support the idea that the complexes exhibit their antitumor activity through a DNA-dependent mechanism of action.

2.3. Interaction with DNA. TEM and confocal studies indicate nuclear localization of **2** and **3**. However they do not modify the electrophoretic mobility of pUC19 plasmid (Figure S24), probably because the compounds in a relatively strong electric field produced during the electrophoresis could dissociate from DNA. Due to the new cationic compounds contain a ligand with increasased π-surface,[83] further studies on

14

DNA interactions of **2** and **3** were undertaken by competitive binding experiments, circular and linear dichroism and viscometry.

2.3.1. Competitive Binding Experiments on Calf thymus DNA. Fluorescence competition experiments with ethidium bromide (EB) are a useful tool to investigate the interaction mode between **2** and **3** with DNA. EB intercalates into DNA, forming a strong emitter adduct ($K_{EB} = 1.2 \times 10^6$ M^{-1})[84] when excited near 520 nm. However, free EB is only weakly fluorescent so that quenching of the EB-DNA fluorescence is used to calculate the magnitude of the interaction between the quencher and DNA.[85,86] The successive additions of **2** to DNA yielded a stronger reduction in the fluorescence at 597 nm than for **3** (Figure S25). As expected, complex **2** ($K_{SV} = 1.9 \times 10^5$ M^{-1}) is a stronger DNA binder than **3** ($K_{SV} = 1.9 \times 10^4$ M^{-1}).[14] The apparent binding constant values (K_{app}) for complexes **2** and **3** were 3.7×10^4 and 1.1×10^4 M^{-1}, respectively (Figures S26 and S27).[85]

2.3.2. Circular and Linear Dichroism Studies. CD spectrometry of ct-DNA treated with **2** or **3** at varying *r* values (*r* = [complex]/[DNA] ratio) was used to investigate how Au(I) complexes bind to DNA and affect its secondary structure (Figure S28). As **2** or **3** are not chiral compounds they yield no intrinsic CD signals. Below 300 nm (where DNA absorbs), alterations in the CD spectra as a consequence of interactions of the DNA with **2** and **3** can be due to disturbances in DNA conformation. As **2** and **3** absorb at the wavelengths lower than 300 nm, the interpretation of CD spectra in terms of alterations in DNA conformation is impossible. The part of the CD spectrum obtained at the wavelengths higher than 300 nm (at ligand transition wavelengths) contains the band corresponding to induced CD due to the interaction of **2** and **3** with a chiral, right-handed structure of DNA. The less intense, broad and positive induced CD bands in the regions of 330−450 nm or 380−450 nm, respectively (Figure S28) are consistent with

specific binding of the Au(I) complexes to DNA.[87] Theoretical calculations have shown that large induced CD signals are expected for groove binding and smaller signals for intercalation.[88] Thus, small induced CD signals of **2** or **3** bound to ct-DNA might be consistent rather with their intercalative DNA binding mode. However, small induced CDs have been also observed for some DNA groove binders in certain positions[89,90] so that the exact orientation of the ligand bound to DNA with respect to the double helix axis based on its induced CD may not be unambiguous.

In this respect flow linear dichroism (LD) has been shown to be more useful than CD. LD (defined as the difference in absorption of light polarized parallel and perpendicular to an orientation axis[91,92] when the sample is subject to flow) was also used for studying the interaction of complexes **2** or **3** with DNA. Flow orientation of DNA molecules (approximately 250 or more base pairs long) can be achieved by Couette flow where two concentric cylinders with a small annular gap (0.5 mm) are aligned and one of them rotates.[93] Absence of a flow LD at the ligand transition wavelengths is generally an indication that the small molecules do not interact with DNA or are bound randomly. On the other hand, the appearance of a ligand LD signal indicates an interaction with DNA and binding in a specific orientation towards DNA. Thus, our observation (Figure 7) that sample of ct-DNA modified with complexes **2** or **3** yielded the LD ligand signals indicates that **2** and **3** may intercalate between the bases of double strands of DNA. The sign of the measured LD at ligand transition wavelengths (at 370−450 nm) and at wavelengths below 300 nm (where DNA absorbs) was negative (Figure 7) which is consistent with DNA remaining in a B-conformation when it interacts with **2** or **3**. More importantly, the negative DNA LD signal at 260 nm is markedly enhanced if even low concentrations of the Au(I) complexes was added (at these loadings the 260 nm LD signal can be completely ascribed to the DNA LD). This increase of DNA LD is usually

connected with either elongation of DNA molecule when it is unwound as a consequence of intercalation or stiffening the DNA. The appearance of weaker negative LD signals at 300−500 nm is consistent with the angle of long axis of the studied complexes to the axis of DNA double helix greater than 54°. This result supports the hypothesis and is consistent with the view that arrangement of the acridine-thiourea moiety of **2** or **3** and the DNA base pairs is coplanar; this arrangement is in agreement with intercalative DNA binding mode.[94]
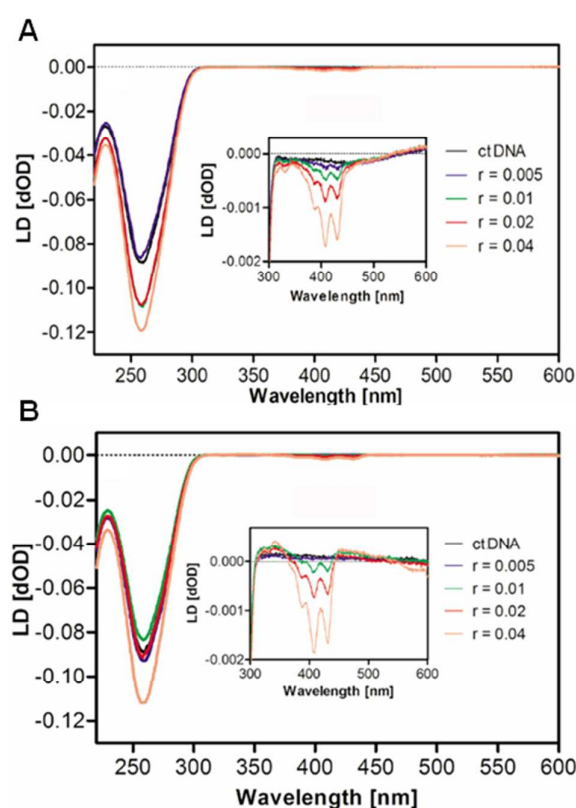
Figure 7. Linear dichroism spectra of ct-DNA (3.5×10^{-4} M) in the presence of increasing concentrations of complexes **2** (A) and **3** (B). Spectra were run in Tris-HCl buffer (10 mM, pH 7.4) at 25 °C.

2.3.3. Viscometry studies. The results of the competition experiments together with flow LD suggest for both compounds intercalative DNA binding mode accompanied by an increase of their rigidity. The classical intercalative DNA binding mode can be

proved by measuring viscosity of DNA samples, which provides information on hydrodynamic properties of DNA.[95] Therefore, the relative specific viscosity of ct-DNA modified by complexes **2** or **3** was examined as well (Figure 8). It has been shown that EB, a well known DNA intercalator, increases the relative specific viscosity as a consequence of its intercalation which results in the increase of persistence length of the DNA molecule. In contrast to EB, the minor-groove binding drugs Hoechst 33258 does not significantly affect viscosity of DNA. Increasing the amounts of **2** or **3** in the reaction with DNA resulted in a continuous increase of the relative viscosity of the DNA, which is consistent with the lengthening of DNA typical for the classical intercalation model.
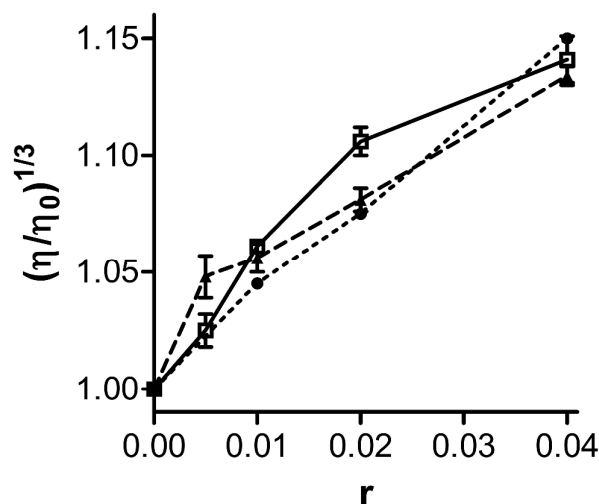

Figure 8. Relative specific viscosity of ct-DNA (3.5×10^{-4} M) in the presence of complex 2 (□) or 3 (▲). Viscosity was measured in Tris-HCl buffer (10 mM, pH 7.4) at 37 °C. As a positive control, relative viscosity of ct-DNA in the presence of intercalator EB (dotted line) is shown. Data represent means ± SD of three separate experiments.

*2.3.4. Emission spectra of complexes **2** and **3** in the presence of different types of DNA.* Since **2** and **3** are fluorescent in DMSO at RT (Figure S10), the possible base-preference was studied by following the changes in their emission spectra after the addition of ct-DNA and the synthetic polynucleotides poly AT and poly GC. Indeed, **2** and **3** exhibit relatively intense emission in buffer (5 mM Tris-HCl, 50 mM NaCl, pH 7) when excited at 390 nm. Upon the addition of either polynucleotide or ct-DNA a strong quenching of the fluorescence of **2** and **3** is observed with little modification of the emission bands position (Figure 9). As stated above the luminiscent properties of **2** and **3** were assigned mainly to IL transitions centered on the ACRTU group and early studies have shown that such excited states are emissive in water and the intensity of the emissions can be diminished on DNA interaction, indicating an intercalative interaction.[83,96] The poly GC and ct-DNA addition results in a significantly more severe fluorescence quenching than poly AT, indicating that both complexes have a higher affinity for GC than AT bases. Although, the affinity of platinum-acridinylthiourea conjugates for the adenines in the minor groove has been previously reported,[97] it is not likely the primary contributor to DNA binding for the Au(I) complexes **2** and **3**.
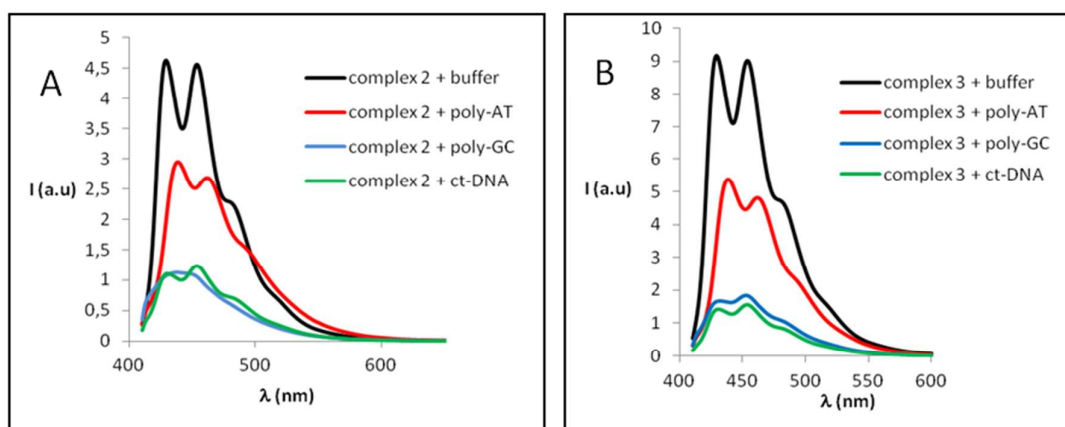
Figure 9. Emission spectra of **2** (A) and **3** (B) in the presence of buffer, poly-AT, poly-GC and calf thymus DNA. [Complexes]: 10 μM, [DNA]: 50 μM, Tris-HCl buffer (pH 7.0), λ_{exc} = 390 nm.

Finally, the possible covalent interaction between the complexes and DNA was also studied by ^{1}H-NMR. Both complexes were incubated in a DMSO-d_6/D$_2$O (1:1) mixture at RT with 9-ethylguanine in 1:5 molar ratio (Figure S29). After 24 h no reaction was observed in the assayed conditions, which suggest that covalent binding is not favored and at the same time support the idea of a non-classical interaction between the Au(I) complexes and DNA.

2.3.5. Inhibition of topoisomerase I (topo I). DNA topoisomerases represent a unique class of enzymes participating in the processes associated with functions of the genome by tuning the level of DNA supercoiling. Moreover, topoisomerase inhibitors have become clinically important targets for cancer chemotherapy treatments.[98-101] and mechanism of action of inhibitors of topo I are often connected with their intercalative DNA binding mode.[102,103]

A DNA-relaxation assay was used to assess the activity of eukaryotic ct topo I in the presence of the Au(I) complexes. The *in vitro* assay for topo I activity was based[104] on monitoring relaxation of negatively supercoiled pSP73KB plasmid in the presence of the Au(I) complexes with the aid of agarose gel electrophoresis. The effect of DNA modification by **2** or **3** on topo I catalyzed DNA relaxation was assessed by comparing the extent of relaxation of nonmodified supercoiled plasmid with plasmid modified by the Au(I) complex.[105] Like other DNA intercalating agents, the Au(I) complexes **2** or **3** exhibited a dose-dependent effect on topo I mediated DNA unwinding (Figure 10). Complex **2** demonstrated somewhat higher inhibitory activity on the relaxation activity

of topo I. Thus, the results of the experiments based on the use of topo I assay are consistent with the view that both complexes **2** or **3** may bind to DNA via intercalation.
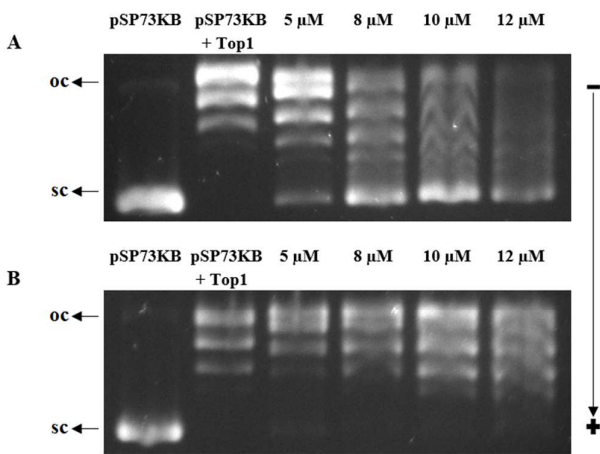
Figure 10. Topo I-mediated relaxation of negatively supercoiled pSP73KB plasmid (6.25 x 10^{-5} M) in the absence or presence of increasing concentrations in the range of 0−12 μM of complexes **2** (A) and **3** (B) analyzed by agarose gel electrophoresis. SC = supercoiled; OC = open circular.

2.4. Inhibition of Tube Formation by Complexes 2 and 3 in EA.hy926 Endothelial Cells. In vitro angiogenesis assays[47,106] were undertaken after incubating EA.hy926 cells for 16 h with **2** and **3** at sub cytotoxic concentrations (Table 1, Figure 11A for **2**). CDDP (1 μM) was used for comparison purposes. The quantification of resulting formation or inhibition of tubular structures was measured (Figures 11B for **2** and Figure S30 for **3**) (μ m^2) .[47]
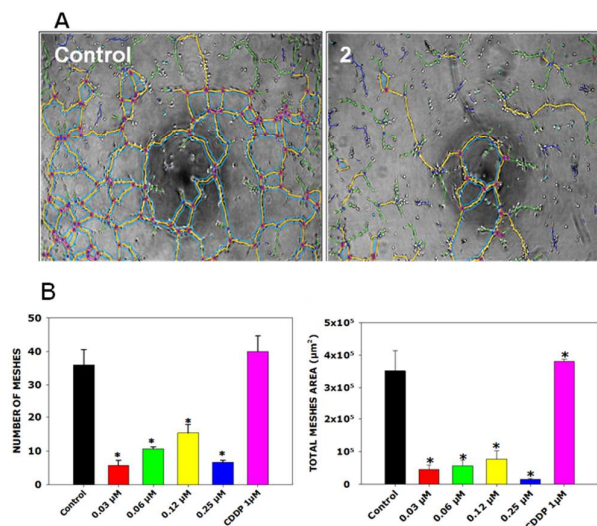
Figure 11. Angiogenesis assay for complex **2**. Typical images after an ImageJ process of EA.hy926 cells (A). Quantification of number of meshes and total meshes area of the capillary structures of EA.hy926 cells treated with compound **2** and CDDP (B). *$p <$ 0.05 was considered to be statistically significant. The results are expressed as mean values ± SD for two independent samples.

Both complexes **2** and **3** inhibit the formation of vascular tubes at 0.25 μM (14 and 4× lower concentration than their IC_{50} in the EA.hy926 cell line, respectively). The inhibitory effect of both compounds remains when a reduction of the concentration until 0.06 μM is carried out. And, it is to be noted that **2** effectively inhibit the tube formation at 0.03 μM, i.e. 119× lower concentration than its IC_{50}. Therefore, inhibition of angiogenesis could contribute to the anticancer capabilities of these compounds. It must take into account that **2** inhibits angiogenesis at 29× lower concentrations than IC_{50} in A2780 cells.

2.5. *In Vitro* Inhibition of Vascular Mimicry in MDA-MB-231 Cells. Highly metastatic MDA-MB-231 cells display the capability to mimic the pattern of embryonic vasculogenic networks found in aggresive tumors, a phenomenon known as

vasculogenic mimicry (VM). Considering the potent antiproliferative activity against metastatic breast cancer as well as the anti-angiogenic activity, we further evaluated the mode of actions of **2** and **3** at sub-IC$_{50}$ concentrations in MDA-MB-231 cells. For that, similar experiments used to study angiogenesis, such as inhibition of tube formation (Figure 12A and 12B) and cell migration were performed (Figure 12C and 12D). The concentration reduction, from 2 to 1 μM, was undertaken in order to completely discard the cytotoxicity effect as responsible of the inhibition. First, tube formation was measured after 16 h incubation and quantified as above. As can be observed in Figure 12B, both complexes significantly inhibited the capillary-like formation structure at 1 μM. Subsequently the wound healing assay[47,107] was carried out for **2** and **3** after treatment for 8 h. Figure 12C shows that **2** diminished the mobility of MDA-MB-231 cells with respect to the control.

Thus, these compounds markedly inhibited capillary-like structure formation and cell migration at concentrations, where no significant cytotoxicity was observed, in MDA-MB-231 cells, indicating that these effects were not due to their antiproliferative and/or proapoptotic effects.
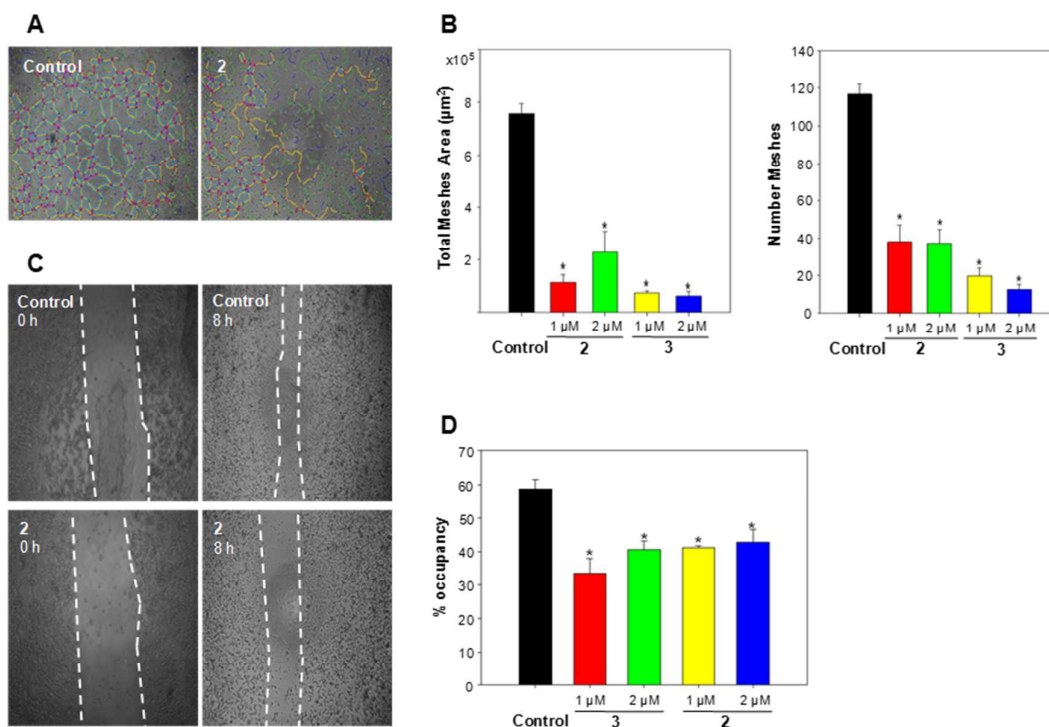
Figure 12. Effect of gold complexes on the development of VM in MDA-MB-231 cells *in vitro*. Typical images after an ImageJ process for culture medium as a control and with **2** (1 μM for 16 h) (A). Quantification of number of meshes and total meshes area of MDA-MB-231 cells treated with **2** and **3** (B). Effect of **2** on the migration of MDA-MB-231 cells. Typical images of the wound at the beginning of the experiment and after 8 h for a control and with **2** (1 μM) (C). % occupancy[47] of **2** and **3** on the migration of MDA-MB-231 cells (D). *$p < 0.05$ was considered to be statistically significant. Error bars indicate ± standard deviations for two sets of three data points for each compound.

3. CONCLUSIONS

Two new monocationic 1-acridin-9-yl-3-methylthiourea Au(I) DNA intercalators [Au(ACRTU)$_2$]Cl (**2**) and [Au(ACRTU)(PPh$_3$)]PF$_6$ (**3**) have been prepared. Both compounds are highly active in cisplatin-sensitive A2780 cells, exhibiting IC$_{50}$ values in the sub-micromolar range. **2** and **3** are also cytotoxic towards the breast tumor cell lines

MDA-MB-231 (triple negative), SK-BR-3 (HER2+, ERα− and ERβ−) and MCF-7 (ER+). We have completed a thorough body of work that contributes to a deeper understanding of the mechanism of action of a potentially interesting class of new anti-cancer agents. Thus, the new compounds increased caspase-3 activity in MCF-7 and MDA-MB231 cells. Compounds **2** and **3** are not able to increase the production of ROS in MCF-7 and MDA-MB-231 cells, the mitochondria membrane potential being unaffected. Ligand **1** and complexes **2** and **3** are strongly emissive in cells, and flow cytometry studies reveal that all of them are able to internalize into cancer cells very quickly. **2** and **3** were localized in the nucleus according to TEM and confocal microscopy in MCF-7 cells. This is in contrast to ligand **1,** which is a strong emitter in the cytosol but surprisingly not in the nucleus. The new complexes were able to bind to DNA via intercalation as shown by spectroscopic methods and viscometry, exhibiting a dose-dependent effect on topoisomerase I mediated DNA unwinding. Additionally, **2** and **3** effectively inhibit angiogenesis in the inmortalized human endothelial cell line EA.hy926 at subcytotoxic concentrations. Furthermore, the new compounds showed vasculogenic mimicry and anti-migratory properties in the highly invasive MDA-MB-231 cell line. In summary, in this work we highlight the value of targeting angiogenesis and vasculogenic mimicry as a strategy for anti-cancer therapy and discuss the benefits of developing small molecules that exhibit these properties in addition to cytotoxicity.

4. EXPERIMENTAL SECTION

Instrumental Measurements. The C, H, N, and S analyses were performed with a Carlo Erba model EA 1108 microanalyzer. Decomposition temperatures were determined with a SDT 2960 simultaneous DSC-TGA of TA instruments Other details of these methods were the same as in the previously published article.[14] Infrared spectra were recorded on a Perkin-Elmer 100 FT-IR spectrometer. The ^{1}H, ^{13}C and ^{31}P spectra

were recorded on a Bruker AV 400 or Bruker AV 600 MHz spectrometer. ESI mass (positive mode) analyses were performed on a HPLC/MS TOF 6220. Absorption spectra were measured with a Varian Cary 4000 UV-Vis spectrophotometer or on a Perkin Elmer Lambda 750 S spectrometer. Fluorescence measurements were carried out with a Perkin Elmer LS 55 50 Hz Fluorescence Spectrometer.

Starting materials and reagents. The starting complex [AuCl(tht)] (tht = tetrahydrothiophene) was prepared by a procedure described elsewhere.[108] The compound [AuCl(PPh$_3$)] was prepared by reacting [AuCl(tht)] with the corresponding phosphine in 1:1 molar ratio in dichloromethane. The 1-acridin-9-yl-3-methylthiourea ligand (ACRTU) **1** was synthesized by using procedures adapted from the literature.[68] Ethidium bromide (EB), Tris-HCl buffer, pUC19 plasmid, and cisplatin [purity $\geq$ 99.9%] were purchased from Sigma-Aldrich. Cisplatin stock solution was prepared by dissolving cisplatin in ultrapure water (Milli-Q$^®$, Merck Millipore) to a final concentration of 3 mM. ct-DNA (42% G + C, mean molecular mass ca. 20 000 kDa) was prepared as previously described.[109,110] Poly-AT (ATATATATATATATATATAT) and poly-GC (GCGCGCGCGCGCGCGCGCGC) were obtained from Eurofins Genomics. The purity of all biologically evaluated molecules, based on elemental analysis, is >95%.

Preparation and Characterization of Au(I) Compounds

Synthesis of [Au(ACRTU)$_2$]Cl (2). [AuCl(tht)] (160 mg, 0.500 mmol) and the thiourea ligand (ACRTU) (267 mg, 1 mmol) were mixed in a 50 mL Schlenck flask. CH$_2$Cl$_2$/MeOH (20 mL, 1:1 v/v) were added. The resulting mixture was stirred at RT for 48 h under nitrogen. The yellow-orange solid was collected by filtration, washed with diethylether and air dried. Yield: 62%. Anal. calcd. for **2** C$_{30}$H$_{26}$N$_6$ClS$_2$Au·CH$_2$Cl$_2$: C,

43.67; H, 3.31; N, 9.86; S, 7.53. Found: C, 44.28; H, 3.41; N, 10.30; S, 7.80. Mp: 204

°C (dec). IR (cm^{-1}): ν(NH) 3219; ν(C=S) 748; ν(Au-S) 452. ^{1}H NMR (400 MHz,

DMSO-d_6, TMS): 13.62 (m, 1 H, NH), 8.54 (m, 1 H, NH), 7.80 (m, 6H, ACRTU), 7.40

(m, 2H, ACRTU), 2.85 (m, 3H, CH$_3$). ^{13}C NMR (100.4 MHz, DMSO-d_6): 173.30,

163.30, 143.27, 138.19, 130.76, 126.95, 121.78, 120.72, 34.85. ESI^{+} mass spectra

(DMSO): m/z +731.13 [C$_{30}$H$_{26}$N$_6$S$_2$Au]$^{+}$. ε_{402} = 23663 M^{-1} cm^{-1} (in DMSO).

Synthesis of [Au(ACRTU)PPh$_3$]PF$_6$ (3). [AuClPPh$_3$] (100 mg, 0.202 mmol) in acetone

(15 mL) was placed in a Schlenck flask under nitrogen, then a solution of AgPF$_6$ (51.14

mg, 0.202 mmol) in acetone (15 mL) was added. AgCl immediately was formed. The

resulting suspension was stirred in the dark for 1 h after which was filtered over a

suspension of thiourea ligand (ACRTU) (54.19 mg, 0.202 mmol) in acetone (20 mL)

under nitrogen. After 3 h stirring, in the dark, the reaction mixed was again filtered

through celite and the solvent was removed under reduced pressure to a minimum.

Diethyl ether was added to precipitate a yellow solid, which was washed with diethyl

ether and dried in vacuo. Yield: 50%. Anal. calcd. for **3** C$_{33}$H$_{28}$N$_3$SP$_2$F$_6$Au: C, 45.48; H,

3.24; N, 4.82; S, 3.68. Found: C, 45.16; H, 3.19; N, 4.74; S, 3.64. Mp: 273 °C (dec). IR

(cm^{-1}): ν(NH) 3418, 3349; (PF$_6$$^-$) 857; ν(C=S) 748; (PPh$_3$) 558-498; ν(Au-S) 452. ^{1}H

NMR (400 MHz, DMSO-d_6, TMS): 12.96 (m, 1H, NH), 9.54 (m, 1 H, <u>NH</u>-CH$_3$), 8.09

(d, 2H, ACRTU, J = 8 Hz), 7.81 (t, 2H, ACRTU, J = 7.2 Hz), 7.57 (m, 4H, ACRTU),

7.41 (m, 9H, PPh$_3$), 6.93 (m, 6H, PPh$_3$), 2.96 (m, 3H, CH$_3$). ^{31}P NMR (121.5 MHz,

DMSO-d_6, H$_3$PO$_4$): 36.81(s, PPh$_3$), -144.14 (sept, PF$_6$, J_{P-F} = 710.87 Hz). ^{13}C NMR

(100.4 MHz, DMSO-d_6): 171.11, 156.54, 139.70, 134.85, 133.28, 132.13, 129.45,

128.01, 127.36, 123.74, 118.33, 116.37, 31.59. ESI^{+} mass spectra (DMSO): m/z

+726.14 [C$_{33}$H$_{28}$N$_3$SPAu]$^{+}$. ε_{402} = 7473 M^{-1} cm^{-1} (in DMSO).

X-ray Crystal Structure Analysis. Suitable crystals of **3** were grown from dichloromethane/hexane. The crystal and molecular structure of **3** have been determined by X-ray diffraction studies (Table S1). A summary of crystal data collection and refinement parameters for compound are given in Tables S1-S3 in the Supporting Information. Crystals were mounted on glass fibers and transferred to the cold gas stream of the diffractometer Bruker SMART D8 Quest using monochromated Mo $K\alpha$ radiation (λ = 0.71073 Å). Absorption corrections were based on multi-scans (program SADABS). Structures were refined anisotropically using SHELXL-97.[111] Hydrogen atoms were included using rigid methyl groups or a riding model, except for H of NH bonds, which were refined freely.

Cell lines and Culture Media. Human breast cancer (MDA-MB-231, SK-BR-3 and MCF-7), pig kidney epithelial LLC-PK1, and EA.hy926 cell lines were acquired from the American Type Tissue Culture Collection (ATCC, USA), while the cell line A2780 was obtained from European Collection of Animal Cell Culture (ECACC, Salisbury, U.K.). This last cell line was cultured in the RPMI-1640 medium, in the Dulbecco's Modified Eagle Medium (DMEM) with a high content of glucose (4.5 g/L), the human breast cancer cells were all cultured in DMEM medium, but with a low glucose (1 g/L) concentration. Finally, LLC-PK1 cells were cultured in the medium M199. All media were supplemented with fetal bovine serum (FBS) 10 %, glutamine 1 mM, and pennicillin and streptomycin. DMEM media was also supplemented with pyruvate 2 mM. Cells were subculture and medium change once a week, and in all case trypsine 0.12%-EDTA 0.05 mM were used. All cell lines were micoplasma-free, as determinated the Hoechts DNA stain method.[112]

Cytotoxicity Assays. Cell proliferation was evaluated by MTT assay in the same way as described in our recently published work.[47] The maximum % of DMSO used was 0.4

1
2
3
4
5
6
7
8
9
10
11
12
13
14
15
16
17
18
19
20
21
22
23
24
25
26
27
28
29
30
31
32
33
34
35
36
37
38
39
40
41
42
43
44
45
46
47
48
49
50
51
52
53
54
55
56
57
58
59
60

(except for CDDP, water diluted) and the measurements were corrected with the corresponding control.

Apoptosis Experiments. The method described elsewhere has been followed.[74] A Beckman Coulter Epics XL flow cytometer was used.

Caspase-3 Assay. MCF-7 and MDA-MB-231 cells were plated in 96-well sterile plates at a density of 1×10^4 cells/well with 200 µL of complete medium and incubated overnight. Then, 1 and 2 µM of compounds **2** and **3** were added for 24 h. For caspase-3 assay, 200 µL of a solution (1 µg/mL) of FITC-DEVD-FMK was added to each well and the plate was incubated for 1 h at 37 °C in the dark. Control cells were not treated with any compound. CDDP (1 µM) was used for comparison purposes. Finally, fluorescence was measured at 535 nm (excitation at 485 nm) in Fluorstar Omega spectrophotometer.

Cell Cycle Arrest Assays. MDA-MB-231 cells (1×10^5) were seeded in 6-well plates and left at 37 °C in a 5% or 10% CO_2 atmosphere for 24 h. After that, the corresponding compound at an IC_{50} concentration was added to each well (except for the control). Cells were incubated in these conditions for 24 h and then, removed from the wells with trypsin-EDTA, collected and centrifuged (250g, 10 min). The supernatant was removed, cells were washed with PBS and centrifuged (250g, 10 min). The supernatant was also removed and the cells treated with EtOH at 70% (phosphate buffered saline, PBS, 30%) for 45 min at 4 ºC and finally EtOH was removed by centrifugation. Cells were resuspended in PBS and finally, RNase solution and PI was added at a final concentration of 0.1 mg/ml and 40 mg/ml, respectively. Cells were incubated in for 30-60 min in this condition, and PI fluorescence was measured for each

cell in a Becton-Dickinson FACSCalibur flow cytometer. In each case 30,000 events were acquired.

Fluorescence Confocal Microscopy Preparations. MCF-7 cells (3×10^4) were seeded in confocal culture dishes and kept in their corresponding culture media at 37 °C for 72 h. Then, compounds **1** (5 μM), **2 (**5 μM) or **3** (2 μM) were added. After 2 h incubation, cells were washed and fixed with 30% MeOH during 30 min. For images shown in Figure 5, the commercial fluorophores DAPI and MitoTracker Red were then added at 100 nM final concentrations. Fixed cells were incubated at 37 °C in these conditions for 30 min. Finally, fluorophores were removed, cells washed twice with PBS and fluorescence was then observed in a confocal fluorescence microscope Espectral Leica TCS SP2. For images shown in Figure S20 no fluorophores were added (concentrations of **2** and **3** used were 5 and 2 μM, respectively).

TEM Sample Preparations. The samples were prepared in the same way as described in our recently published work.[47]

Metal Cellular Accumulation Studies. Cellular accumulations of **2**, **3** and CDDP were determined in A2780 human ovarian carcinoma cells in the same way as described in our recently published work.[75]**Internalization of 1−3 in living cells using flow cytometry.** A2780 and MCF-7 cells (10^5 cells/well) in complete medium were seeded in 6 well/plate and incubated at 37 °C for 24 h under a 5% CO_2 humidify atmosphere. Then, cells were incubated at different times with **1-3** at concentration 5 µM, washed with PBS and detached by trypsin 0.12%-EDTA 0.05 mM. The suspended cell solution was collected by centrifugation at 200g for 5 min and further washed with PBS three times. Flow cytometry was performed using a FACSCalibur flow cytometer (Becton Dickinson & Co., Franklin Lakes, NJ). Control cells without any treatment were used to

set the gating. The samples were collected in FL1 channel. Each measurement set was performed using 10,000 cells.

Measurement of the Partition Coefficients. To determine the partition coefficients (P) of tested compounds, the "shake flask" method was used in the same way as described in our previously published article. [113] All estimations were done in triplicate, each made in quadruplicate.

RP-HPLC/MS Determinations. Relative hydrophobicity measurements were performed using a RP-HPLC/MS TOF 6220. Chromatographic analyses were carried out on a Brisa C18 column (150 mm × 4.6 mm, 5 μm particle size). The mobile phase was a mixture of (A) H_2O/HCOOH 0.1% and (B) acetonitrile/HCOOH 0.1%. The flow rate was 0.6 mL min^{-1} in a linear gradient starting with 10% B at 0–13 min, reaching 90% B at 14–20 min, and 10% B at 21–25 min. Chromatograms were recorded at 280 nm. The HPLC system was controlled by a ChemStation software (MASS HUNTER). Samples were dissolved in DMF (1 mg/mL final concentration).

Intracellular Reactive Oxygen Species (ROS) Determination. Intracellular ROS were quantified to determine the oxidative stress after the treatment with 1 or 2 μM of **2** and **3** for 12 h in MCF-7 and MDA-MB-231 cells. Both cell lines (1×10^4 cells/well) were seeded on 96-well plates and left attached overnight. The treated cells were loaded with 25 μM DCFH-DA and incubated for 45 min at 37 °C before adding the compounds. Untreated cells containing maximal concentration of DMSO used in the treatment (0.4%) were used as a control. Fluorescence was measured on Fluostar Galaxy spectrophotometer (excitation/ emission wavelengths: 485 nm/535 nm).

Mitochondrial Polarization Assay. Briefly, cells were seeded at 1×10^4 cells/well in 96-well plates and left to incubate overnight. Compounds **2**, **3** and CDDP were added at

31

a final concentration of 1 or 2 μM and the cells were left to incubate for 24 h. Cells were collected, washed twice with PBS and 1 μL/mL of a solution of Rho123 (1 mM, Sigma Aldrich) was added to each sample. Samples were incubated 15 min and immediately analyzed on a FACSCalibur cytometer. In all case 10,000 events were analyzed.

Gel electrophoretic mobility of pUC19 plasmid. Compounds **2** and **3** were serially diluted 1:2 in the presence of 40 μg/mL pUC19 plasmid DNA in 10 mM phosphate buffer, pH 7.4, and incubated overnight at 37 °C prior to gel electrophoresis. DNA control samples and gel electrophoresis were performed following a previously reported procedure.[114] In brief, samples were resolved on a 1% agarose gels prepared in tris-acetate buffer with 0.3 μg of plasmid/lane. The gels were stained with 0.5 μg mL^{-1} EB in tris-acetate buffer at RT for 40 min, destained with tris-acetate buffer, and imaged on an ALPHAIMAGER EC (Alpha Innotech).

Ethidium bromide displacement experiments. They were undertaken in the same way as described in our recently published work.[47]

Circular and Flow Linear Dichroism Spectroscopy. Isothermal CD spectra of ct-DNA at the concentration of 0.112 mg mL^{-1} (3.5×10^{-4} M in nucleotides) modified by **2** or **3** at r in the range of 0.005−0.08 were recorded at 25 °C in Tris-HCl (10 mM, pH 7.4) using a Jasco J-720 spectropolarimeter (r is defined as the molar ratio of free Au(I) complex to nucleotide phosphates at the onset of incubation with DNA). LD spectra were recorded by means of a flow Couette cell in a Jasco J-720 dichrograph adapted for LD measurements. Other details of these methods were the same as in the previously published article.[115]

Viscometry. The relative viscosity of the solutions of ct-DNA [0.112 mg mL^{-1} (3.5 × 10^{-4} M in monomeric nucleotides)] was measured using AMVn Automated Micro Viscometer (Anton Paar GmbH, Austria). Other details were the same as in the previously published work. [115]

Emission spectra of complexes 2 and 3 in the presence of different types of DNA. The emission of **2** and **3** at 10 μM were tested in the presence of 50 μM of each DNA given in Table S4 of the Supporting Information in a 500 μL quartz cuvette. 1% DMSO was used to ensure completely disolution of complexes. For DNA sequences the concentration is measured in bases of pairs [bp] and the ratio of [Au]/[bp] was 1:5. A final volume of 300 μL was used for all samples.[116] Data collection was taken before and after the addition of DNA and the emission spectra were recorded in the wavelength range 370–720 nm by exciting at λ_{ex} = 390 nm.

Inhibition of Topoisomerase I. Negatively supercoiled pSP73KB plasmid (2455 bp) was used to investigate how the binding of **2** and **3** affects the relaxation of supercoiled DNA with topoI. Each sample (10 μL) contained DNA (0.2 μg, control or DNA modified by the Au(I) complex) in Tris-HCl (35 mM, pH 8.0), KCl (72 mM), MgCl$_2$ (5 mM), dithiothreitol (DTT) (5 mM), spermidine (5 mM), BSA (0.01%) and ct topoisomerase I (topo I) (0.4 unit, 1 U/0.5 μg DNA). ct topoI was from Takara, Japan. The samples were incubated for 1 h at 37 °C and analyzed by agarose gel electrophoresis. SYBR$^®$ Green I (Molecular Probes^{TM}, Eugene, OR) diluted 1:10000 in 1 × TAE buffer was used to stain the gels which were visualized by UV-light. Other details of this method were the same as in the previously published article.[101]

Endothelial Tube Formation Assay. In the same way as described in our recently published work.[47]

Vascular mimicry capillary-like structure formation by MDA-MB-231 breast cancer assay. MDA-MB-231 cells (12×10^3 cells/well) were seeded in complete medium on polymerized Matrigel matrix (9 μL/well, 8.7 mg/mL; B&D Biosciences, Bedford, MA) in 96-well plates. After 16 h incubation, cells exposed to 1 or 2 μM of complex **2** and **3** the wells were photographed using an inverted phase-contrast microscope (Nikon mod. Eclipse TE-2000-U). Capillary-like structure was quantified by measuring the number and area of meshes under 4× magnification using ImageJ software (National Institutes of Health, Bethesda, MD, USA).

Wound healing Assay (Scracth test). In the same way as described in our recently published work.[47]

Statistical Analysis. To compare independent groups of numerical data ANOVA test was used. All statistical analyses were performed using SigmaPlot v.11. *p <0.05 was statically significant.

Supporting Information. Additional NMR, absorption and emission fluorescence spectra, RP-HPLC chromatograms, figures for cell cycle analysis, apoptosis, caspase-3 activation, ROS level, mitochondrial membrane potential, agarose gels of pUC19 plasmid and circular dichroism spectra (PDF), and crystallographic data and file for **3** (CIF). This material is available free of charge via the Internet at http://pubs.acs.org.

AUTHOR INFORMATION

Corresponding Author

*E-mail: jruiz@um.es. Fax: +34 868 884148. Tel: +34 868 887455

ORCID

José Ruiz: 0000-0002-0834-337X

Author Contributions

The manuscript was written through contributions of all authors. All authors have given approval to the final version of the manuscript.

REFERENCES

(1) Alessio E., ed. Bioinorganic Medicinal Chemistry, Weinheim, Wiley-VCh, 2011.

(2) Jaouen G. and Metzler-Nolte N. Medicinal organometallic chemistry. Topics in Organometallic Chemistry, Springer-Verlag, 2010.

(3) Teoh, D. G., Secord, A. A. (2011) Antiangiogenic therapies in epithelial ovarian cancer. *Cancer Control*, *18*, 31–43.

(4) Barry, N. P. E, Sadler, P. J. **(**2013) Exploration of the medical periodic table: towards new targets. *Chem. Commun. 49*, 5106–5131.

(5) Wang, D., Lippard, S. J. (2005) Cellular processing of platinum anticancer drugs. *Nat. Rev. Drug Discov.*, *4*, 307–320.

(6) Kelland, L. R. (2007) The resurgence of platinum-based cancer chemotherapy. *Nat. Rev. Cancer 7*, 573–584.

(7) Kelland, L. R. (2000) Preclinical perspectives on platinum resistance. *Drugs 59*, 1–8.

(8) Ott, I., Gust. R. (2007) Non platinum metal complexes as anti-cancer drugs. *Arch. Pharm. 340*, 117–126.

(9) Gasser, G., Ott, I., Metzler-Nolte, N. (2011) Organometallic anticancer compounds. *J. Med. Chem. 54*, 3−25.

(10) Yellol, J., Pérez, S. A., Buceta, A., Yellol, G., Donaire, A., Szumlas P, Bednarski P. J., Makhloufi, G., Janiak, C., Espinosa, A., Ruiz, J. (2015) Novel C,N-Cyclometalated Benzimidazole Ruthenium(II) and Iridium(III) Complexes as Antitumor and Antiangiogenic Agents: A Structure-Activity Relationship Study. *J. Med. Chem.*, *58*, 7310–7327.

(11) Yellol, J., Pérez, S. A., Yellol, G., Zajac, J., Donaire, A., Vigueras, G., Novohradsky, V., Janiak, C., Brabec, V., Ruiz, J. (2016) Highly potent extranuclear-targeted luminescent iridium(III) antitumor agents containing benzimidazole-based ligands with a handle for functionalization. *Chem. Commun. 52*, 14165-14168.

(12) Wachter, E., Zamora, A., Nease, L., Heidary, D. K., Ruiz, J., Glazer, E. C. (2016) Geometry matters: inverse cytotoxic relationship for cis/trans-Ru(II) polypyridyl complexes from cis/trans-[PtCl$_2$(NH$_3$)$_2$]. *Chem. Comm. 52*, 10121-10124.

(13) Zamora, A., Denning, C. A., Heidary, D. K., Wachter, E., Nease, L.A., Ruiz, J., Glazer, E.C. (2017) Ruthenium-containing P450 inhibitors for dual enzyme inhibition and DNA damage. *Dalton Trans.*, *46*, 2165-2173.

(14) Ruiz, J., Vicente, C., de Haro, C., Bautista, D. (2013) Novel Bis-C,N-Cyclometalated Iridium(III) Thiosemicarbazide Antitumor Complexes: Interactions with Human Serum Albumin and DNA, and Inhibition of Cathepsin B.. *Inorg. Chem.*, *52*, 974-982.

(15) Tiekink, E. R. (2008) Anti-cancer potential of gold complexes. *Inflammopharmacology 16*, 138–142.

(16) Che, C.-M., Siu, F.-M. (2010) Metal complexes in medicine with a focus on enzyme inhibition. *Curr. Opin. Chem. Biol. 14*, 255–261.

(17) Zou,T., Lum, C. T., Chui, S.-Y., Che, C.-M. (2013**)** Gold(III) complexes containing N-heterocyclic carbene ligands: thiol "switch-on" fluorescent probes and anti-cancer agents. *Angew. Chem. Int. Ed. 52*, 2930–2933.

(18) Ronconi, L., Giovagnini, L., Marzano, C., Bettìo, F., Graziani, R., Pilloni, G., Fregona, D. (2005) Gold dithiocarbamate derivatives as potential antineoplastic agents: design, spectroscopic properties, and in vitro antitumor activity. *Inorg. Chem. 44*, 1867–1881.

(19) Liu, W., Gust, R. (2013) Metal N-heterocyclic carbene complexes as potential antitumor metallodrugs. *Chem. Soc. Rev. 42*, 755–773.

(20) Casini, A., Messori, L. (2011) Molecular mechanisms and proposed targets for selected anticancer gold compounds. *Curr. Top. Med. Chem. 11*, 2647–2660.

(21) Bertrand, B., Casini, A. (2014) A golden future in medicinal inorganic chemistry: the promise of anticancer gold organometallic compounds. *Dalton Trans. 43*, 4209–4219.

(22) Ott, I. (2009) On the medicinal chemistry of gold complexes as anticancer drugs. *Coord. Chem. Rev. 253*, 1670–1681.

(23 Berners-Price, S. J., Filipovska, A. (2011) Gold compounds as therapeutic agents for human diseases. *Metallomics 9*, 863–873.

(24) Cutillas, N., Yellol, G. S., de Haro, C., Vicente, C., Rodríguez, V., Ruiz, J. (2013) Anticancer cyclometalated complexes of platinum group metals and gold. *Coord. Chem. Rev. 257*, 2784–2797.

(25) Ortego, L., Cardoso, F., Martins, S., Fillat, M. F., Laguna, A., Meireles, M., Villacampa, M. D., Gimeno, M. C. (2014) Strong inhibition of thioredoxin reductase by highly cytotoxic gold(I) complexes. DNA binding studies. *J. Inorg Biochem. 130*, 32–37.

(26) Medici, S., Peana, M., Nurchi, V. M., Lachowicz, J. I., Crisponi, G., Zoroddu, M. A. (2015) Noble metals in medicine: latest advances. *Coord. Chem. Rev. 284*, 329–350.

(27) Che, C.-M., Sun, R. W. (2011) Therapeutic applications of gold complexes: lipophilic gold(III) cations and gold(I) complexes for anti-cancer treatment. *Chem. Commun. 47*, 9554–9560.

(28) Gutiérrez, A., Marzo, I., Cativiela, C., Laguna, A., Gimeno, M. C. (2015) Highly cytotoxic bioconjugated gold(I) complexes with cysteine-containing dipeptides. *Chem. Eur. J. 21*, 11088–11095.

(29) Doulain, P. E., Decréau, R., Racoeur, C., Goncalves, V., Dubrez, L., Bettaieb, A., Le Gendre, P., Denat, F., Paul, C., Goze, C., Bodio, E. (2015) Towards the elaboration of new gold-based optical theranostics. *Dalton Trans. 44*, 4874–4883.

(30) Meyer, A., Bagowski, C. P., Kokoschka, M., Stefanopoulou, M., Alborzinia, H., Can, S., Vlecken, D. H., Sheldrick, W. S., Wölfl, S., Ott, I. (2012) On the biological properties of alkynyl phosphine gold(I) complexes. *Angew. Chem. Int. Ed. 51*, 8895–8899.

(31) Tiekink, E. R. (2003) Phosphine gold(I) thiolates: pharmacological use and potential. *Bioinorg. Chem. Appl.* 53–67.

(32) Hickey, J. L., Ruhayel, R. A., Barnard, P. J., Baker, M. V., Berners-Price, S. J., Filipovska, A. (2008) Mitochondria-targeted chemotherapeutics: the rational design of gold(I) N-heterocyclic carbene complexes that are selectively toxic to cancer cells and target protein selenols in preference to thiols. *J. Am. Chem. Soc. 130*, 12570–12571.

(33) Baker, M. V., Barnard, P. J., Berners-Price, S. J., Brayshaw, S. K., Hickey, J. L., Skelton, B. W., White, A. H. (2006) Cationic, linear Au(I) N-heterocyclic carbene complexes: synthesis, structure and anti-mitochondrial activity. *Dalton Trans.* 3708–3715.

(34) Ott, I., Qian, X., Xu, Y., Vlecken, D. H., Marques, I. J., Kubutat, D., Will, J., Sheldrick, W. S., Jesse, P., Prokop, A., Bagowski, C. P. (2009) A gold(I) phosphine complex containing a naphthalimide ligand functions as a TrxR inhibiting antiproliferative agent and angiogenesis inhibitor. *J. Med. Chem. 52*, 763–770.

(35) Rubbiani, R., Salassa, L., de Almeida, A., Casini, A. and Ott, I. (2014) Cytotoxic Gold(I) N-heterocyclic Carbene Complexes with Phosphane Ligands as Potent Enzyme Inhibitors. *ChemMedChem 9*, 1205–1210.

(36) Yang, M., Pickard, A. J., Qiao, X., Gueble, M. J., Day, C. S., Kucera, G. L., Bierbach, U. (2015) Synthesis, reactivity, and biological activity of gold(I) complexes modified with thiourea-functionalized tyrosine kinase inhibitors. *Inorg. Chem. 54*, 3316−3324.

(37) Yan K, Lok C.-N., Bierla, K., Che, C.-M. (2010) Gold(I) complex of N,N'-disubstituted cyclic thiourea with in vitro and in vivo anticancer properties-potent tight-binding inhibition of thioredoxin reductase. *Chem. Commun. 46*, 7691–7693.

(38) Ronconi, L., Marzano, C., Zanello, P., Corsini, M., Miolo, G., Maccà, C., Trevisan, A., Fregona, D. (2006) Gold(III) dithiocarbamate derivatives for the treatment of

cancer: solution chemistry, DNA binding, and hemolytic properties. *J. Med. Chem. 49*, 1648–1657.

(39) Casini, A., Cinellu, M. A., Minghetti, G., Gabbiani, C., Coronnello, M., Mini, E., Messori, L. (2006) Structural and solution chemistry, antiproliferative effects, and DNA and protein binding properties of a series of dinuclear gold(III) compounds with bipyridyl ligands. *J. Med. Chem. 49*, 5524–5531.

(40) Yan, J. J., Chow, A. L.-F., Leung, C.-H, Sun, R. W.-Y., Ma, D.-L., Che, C.-M. (2010) Cyclometalated gold (III) complexes with N-heterocyclic carbene ligands as topoisomerase I poisons. *Chem. Commun. 46*, 3893–3895.

(41) Chin, C. (2016) Future options of anti-angiogenic cancer therapy; *J. Cancer 35*, 21

(42) Maj, E., Papiernik, D., Wietrzyk, J. (2016) Antiangiogenic cancer treatment: The great discovery and greater complexity. *Int. J. Oncol.49*, 5, 1773–1784.

(43) Folkman, J. (2004) Endogenous angiogenesis inhibitors. *APMIS 112*, 496–507.

(44) Aranda, E., Owen, G. I. (2009) A semi-quantitative assay to screen for angiogenic compounds and compounds with angiogenic potential using the EA.hy926 endothelial cell line. *Biol. Res. 42*, 377–389.

(45) Ma, J., Waxman, D. J. (2008) Combination of antiangiogenesis with chemotherapy for more effective cancer treatment. *Mol. Cancer Ther. 7*, 3670–3684.

(46) Teoh, D. G., Secord, A. A. (2011) Antiangiogenic therapies in epithelial ovarian cancer. *Cancer Control 18*, 31–43.

(47) Zamora, A., Pérez, S. A., Rodríguez, V., Janiak, C., Yellol, G., Ruiz, J. (2015) Dual antitumor and antiangiogenic activity of organoplatinum(II) complexes. *J. Med. Chem. 58,* 1320-1336.

(48) Rademaker-Lakhai, J. M., van den Bongard, D., Pluim, D., Beijnen, J. H., Schellens, J. H. (2004) A Phase I and pharmacological study with imidazolium-trans-DMSO-imidazole-tetrachlororuthenate, a novel ruthenium anticancer agent. *Clin. Cancer Res. 10*, 3717–3727.

(49) Yang, L., Zhang, J., Wang, C., Qin, X., Yu, Q., Zhou, Y., Liu, J. (2014) Interaction between 8-hydroxyquinoline ruthenium(II) complexes and basic fibroblast growth factors (bFGF): inhibiting angiogenesis and tumor growth through ERK and AKT signaling pathways. *Metallomics 6*, 518–531.

(50) Nowak-Sliwinska, P., van Beijnum, J. R., Casini, A., Nazarov, A. A., Wagnières, G., van den Bergh, H., Dyson, P. J., Griffioen, A. W. (2011) Organometallic

ruthenium(II) arene compounds with antiangiogenic activity. *J. Med. Chem. 54*, 3895–3902.

(51) Liu, L.-J., Lin, S., Chan, D. S.-H., Vong, C. T., Hoi, P. M., Wong, C.-Y., Ma, D.-L., Leung, C.-H. (2014) A rhodium(III) complex inhibits LPS-induced nitric oxide production and angiogenic activity *in cellulo*. *J. Inorg. Biochem. 140,* 23–28.

(52) Wilbuer, A., Vlecken, D. H., Schmitz, D. J., Kräling, K., Harms, K., Bagowski, C. P., Meggers, E. (2010) Iridium complex with antiangiogenic properties. *Angew. Chem. Int. Ed. 49*, 3839–3842.

(53) Nazarov, A. A., Baquié, M., Nowak-Sliwinska, P., Zava, O., van Beijnum, J. R., Groessl, M., Chisholm, D. M., Ahmadi, Z., McIndoe, J. S., Griffioen, A. W., van den Bergh, H., Dyson, P. J. (2013**)** Synthesis and characterization of a new class of anti-angiogenic agents based on ruthenium clusters. *Sci. Rep. 3*, 1485.

(54) Sun, R. W.-Y., Ng, M. F.-Y., Wong, E. L.-M., Zhang, J., Chui, S. S.-Y., Shek, L., Lau, T.-C., Che, C.-M. (2009) Dual anti-angiogenic and cytotoxic properties of ruthenium(III) complexes containing pyrazolato and/or pyrazole ligands. *Dalton Trans*. 10712–10716.

(55) Zhang, J.-J., Sun, R. W.-Y., Che, C.-M. (2012) A dual cytotoxic and anti-angiogenic water-soluble gold(III) complex induces endoplasmic reticulum damage in HeLa cells. *Chem. Commun*, *48*, 3388–3390.

(56) Clavel, C. M., Păunescu, E., Nowak-Sliwinska, P., Griffioen, A. W., Scopelliti, R., Dyson, P. J. (2014) Discovery of a highly tumor-selective organometallic ruthenium(II)–arene complex. *J. Med. Chem. 5*7, 3546–3558.

(57) Muenzner, J. K., Rehm, T., Biersack, B., Casini, A., de Graaf, I. A., Worawutputtapong, P., Noor, A., Kempe, R., Brabec, V., Kasparkova, J., Schobert, R. (2015) Adjusting the DNA interaction and anticancer activity of Pt(II) N-heterocyclic carbene complexes by steric shielding of the trans leaving group. *J. Med. Chem. 58*, 6283–6292.

(58) Muenzner, J. K., Biersack, B., Kalie, H., Andronache, I. C., Kaps, L., Schuppan, D., Sasse, F., Schobert, R. (2014) Gold(I) Biscarbene Complexes Derived from Vascular-Disrupting Combretastatin A-4 Address Different Targets and Show Antimetastatic Potential. *Chem. Med. Chem. 9*, 1195–1204.

(59) Maniotis, A. J., Folberg, R., Hess A., Seftor, E. A., Gardner, L. M., Pe'er, J., Trent, J. M., Meltzer, P. S., Hendrix, M. J. (1999) Vascular channel formation by human

melanoma cells in vivo and in vitro: vasculogenic mimicry. *Am. J. Pathol. 155*, 739–752.

(60) Liu, X., Wang, X., Du, W., Chen, L., Wang, G., Cui, Y., Liu, Y., Dou, Z., Wang, H., Zhang, P., Chang, L., Yi, L., Cai, J., Jiang, C. (2014) Suppressor of fused (Sufu) represses Gli1 transcription and nuclear accumulation, inhibits glioma cell proliferation, invasion and vasculogenic mimicry, improving glioma chemo-sensitivity and prognosis. *Oncotarget. 5*, 11681–11694.

(61) Kobayashi, H., Shirakawa, K., Kawamoto, S., Saga, T., Sato, N., Hiraga, A., Watanabe, I., Heike, Y., Togashi, K., Konishi, J., Brechbiel, M. W., Wakasugi, H. (2002) Rapid accumulation and internalization of radiolabeled herceptin in an inflammatory breast cancer xenograft with vasculogenic mimicry predicted by the contrast-enhanced dynamic MRI with the macromolecular contrast agent G6-(1B4M-Gd)(256). *Cancer Res. 62*, 860–866.

(62) Shirakawa, K., Kobayashi, H., Heike, Y., Kawamoto, S., Brechbiel, M. W., Kasumi, F., Iwanaga, T., Konishi, F., Terada, M., Wakasugi, H. (2002) Hemodynamics in Vasculogenic mimicry and angiogenesis of inflammatory breast cancer xenograft. *Cancer Res. 62*, 560–566.

(63) Shirakawa, K., Kobayashi, H., Sobajima, J., Hashimoto, D., Shimizu, A., Wakasugi, H. (2003) Inflammatory breast cancer: vasculogenic mimicry and its hemodynamics of an inflammatory breast cancer xenograft model. *Breast Cancer Res. 5*, 136–139.

(64) Ebos, J. M., Lee, C. R., Cruz-Munoz, W., Bjarnason, G. A., Christensen, J. G., Kerbel, R. S. (2009) Accelerated metastasis after short-term treatment with a potent inhibitor of tumor angiogenesis. *Cancer Cell 15*, 232–239.

(65) Cao, Z., Bao, M., Miele, L., Sarkar, F. H., Wang, Z., Zhou, Q. (2013) Tumour vasculogenic mimicry is associated with poor prognosis of human cancer patients: A systemic review and meta-analysis. *Eur. J. Cancer 49*, 3914–3923.

(66) Cui, Y. F., Liu, A. H., An, D. Z., Sun, R. B., Shi, Y., Shi, Y. X., Shi, M., Zhang, Q., Wang, L. L., Feng, Q., Pan, G. L., Wang, Q. (2015) Claudin-4 is required for vasculogenic mimicry formation in human breast cancer cells. *Oncotarget 6*, 11087–11097.

(67) Suryadi, J., Bierbach, U. (2012) DNA metalating-intercalating hybrid agents for the treatment of chemoresistant cancers. *Chem. Eur. J. 18*, 12926–12934.

(68) Martins, E., Baruah, H., Kramarczyk, J., Saluta, G., Day, C. S., Kucera, G. L., Bierbach U. (2001) Design, synthesis, and biological activity of a novel non-cisplatin-type platinum-acridine pharmacophore. *J. Med. Chem. 44*, 4492–4496.

(69) Eiter, L. C., Hall, N. W., Day, C. S., Saluta, G., Kucera, G. L., Bierbach, U. (2009) Gold(I) analogues of a platinum-acridine antitumor agent are only moderately cytotoxic but show potent activity against Mycobacterium tuberculosis. *J. Med. Chem. 52*, 6519–6522.

(70) Salvesen, G. S., Riedl, S. J. (2008) Caspase mechanisms. *Adv. Exp. Med. Biol. 615*, 13−23.

(71) Choi, J. A., Kim, J. Y., Lee, J. Y., Kang, C. M., Kwon, H. J., Yoo, Y. D., Kim, T. W., Lee, Y. S., Lee, S. J. (2001) Induction of cell cycle arrest and apoptosis in human breast cancer cells by quercetin. *Int. J. Oncol. 19,* 837–844.

(72) Dighe, S. U., Khan, S., Soni, I., Jain, P., Shukla, S., Yadav, R., Sen, P., Meeran, S. M., Batra, S. (2015) Synthesis of β-Carboline-Based N-Heterocyclic Carbenes and Their Antiproliferative and Antimetastatic Activities against Human Breast Cancer Cells. *J. Med. Chem. 58*, 3485-3499.

(73) Imstepf, S., Pierroz,,V., Raposinho, P., Bauwens, M., Felber, M., Fox, T., Shapiro, A. B., Freudenberg, R., Fernandes, C., Gama, S., Gasser, G., Motthagy, F., Santos, I. R., Alberto, R. (2015) Nuclear Targeting with an Auger Electron Emitter Potentiates the Action of a Widely Used Antineoplastic Drug. *Bioconjugate Chem. 26*, 2397–2407.

(74) Lozano-Pérez, A., Gil, A. L., Pérez, S. A., Cutillas, N., Meyer, H., Pedreño, M., Aznar-Cervantes, S., Janiak, C., Cenis, J.L., Ruiz, J. (2015) Antitumor Properties of Platinum(IV) Prodrug-Loaded Silk Fibroin Nanoparticles. *Dalton Trans. 44*, 13513-13521.

(75) Zajac, J., Kostrhunova, H., Novohradsky, V., Vrana, O., Raveendran R., Gibson, D., Kasparkova J., Brabec, V. (2016) Potentiation of mitochondrial dysfunction in tumor cells by conjugates of metabolic modulator dichloroacetate with a Pt(IV) derivative of oxaliplatin. *J. Inorg. Biochem. 156*, 89–97.

(76) Millett, A. J., Habtemariam, A., Romero-Canelón, I., Clarkson, G. J., Sadler, P. J. (2015) Contrasting Anticancer Activity of Half-Sandwich Iridium(III) Complexes Bearing Functionally Diverse 2‑Phenylpyridine Ligands. *Organometallics 34*, 2683–2694.

(77) Novohradsky, V., Zerzankova, L., Stepankova, J., Kisova, A., Kostrhunova, H., Liu, Z., Sadler, P. J., Kasparkova, J., Brabec, V. (2014) A dual-targeting, apoptosis-inducing organometallic half-sandwich iridium anticancer complex. *Metallomics 6*, 1491−1501.

(78) Robinson, J. P., Bruner, L. H., Bassoe, C. F., Hudson, J. L., Ward, P. A., Phan, S. H. (1988) Measurement of intracellular fluorescence of human-monocytes relative to oxidative metabolism. *J. Leukocyte Biol. 43*, 304−310.

(79) Kalyanaraman, B., Darley-Usmar, V., Davies, K. J., Dennery, P. A., Forman, H. J., Grisham, M. B., Mann, G. E., Moore, K., Roberts, L. J., Ischiropoulos, H. (2012) Measuring reactive oxygen and nitrogen species with fluorescent probes: challenges and limitations. *Free Radical Biol. Med. 52*, 1−6.

(80) Chen, L. B. (1988) Mitochondrial membrane potential in living cells. *Annu. Rev. Cell Biol. 4*, 155−181.

(81) Yoong, S. L., Wong, B. S., Zhou, Q. L., Chin, C. F., Li, J., Venkatesan, T., Ho, H. K., Yu, V., Ang, W. H., Pastorin, G. (2014) Enhanced cytotoxicity to cancer cells by mitochondria-targeting MWCNTs containing platinum(IV) prodrug of cisplatin. *Biomaterials 35*, 748−759.

(82) Ke, S. Z., Ni, X. Y., Zhang, Y. H.; Wang, Y. N., Wu, B., Gao, F. G. (2013) Camptothecin and cisplatin upregulate ABCG2 and MRP2 expression by activating the ATM/NF-κB pathway in lung cancer cells. *Int. J. Oncol. 42*, 1289−1296.

(83) Stimpson, S., Jenkinson, D. R., Sadler, A., Latham, M., Wragg, A., Meijer, A. J., Thomas, J. A. (2015) Tuning the excited state of water-soluble Ir(III)-based DNA intercalators that are isostructural with [Ru(II)(NN)$_2$(dppz)] Light-Switch Complexes. *Angew. Chem. Int. Ed. 54*, 3000–3003.

(84) Peberdy, J. P., Malina, J., Khalid, S., Haman, M. J., Rodger, A. (2007) Influence of surface shape on DNA binding of bimetallo helicates. *J. Inorg. Biochem. 101*, 1937−1945.

(85) Beckford, F., Dourth, D., Shaloski, M. Jr, Didion, J., Thessing, J., Woods, J., Crowell, V., Gerasimchuck, N., Gonzalez-Sarrías, A., Seeram, N. P. (2011) Half-sandwich ruthenium–arene complexes with thiosemicarbazones: synthesis and biological evaluation of [(η^6-p-cymene)Ru(piperonal thiosemicarbazones)Cl]Cl complexes. *J. Inorg. Biochem. 105*, 1019−1029.

(86) Beckford, F., Thessing, J., Woods, J., Didion, J., Gerasimchuck, N., Gonzalez-Sarrías, A., Seeram, N. P. (2011) Synthesis and structure of [(η^6-p-cymene)Ru(2-anthracen-9-ylmethylene-N-ethylhydrazinecarbothioamide)Cl]Cl; biological evaluation, topoisomerase II inhibition and reaction with DNA and human serum albumin. *Metallomics 3*, 491−502.

(87) Caesar, C. E. B., Johnsson, R., Ellervik, U., Fox, K., R., Lincoln, P., Norden, B. (2006) A polarized-light spectroscopy study of interactions of hairpin polyamide with DNA. *Biophys. J. 91*, 904–911.

(88) Norden, B., Lincoln, P., Akerman, B., Tuite, E. In Sigel, A. and Sigel, H. (eds.). *Metal Ions in Biological Systems: Probing of Nucleic Acids by Metal Ion Complexes of Small Molecules*. Marcel Dekker, Inc., New York, Basel, Hong Kong, 1996, Vol. 33, pp. 177–252.

(89) Lyng, R., Rodger, A., Norden, B. (1991) The CD of ligand-DNA systems. 1. Poly(dG-dC) B-DNA. *Biopolymers 31*, 1709–1720.

(90) Lyng, R., Rodger, A., Norden, B. (1992) The CD of ligand-DNA systems. 2. Poly(dA-dT) B-DNA. *Biopolymers 32*, 1201–1214.

(91) Marrington, R., Dafforn, T. R., Halsall, D. J., and Rodger, A. (2004) Micro-volume Couette flow sample orientation for absorbance and fluorescence linear dichroism, *Biophys. J. 87*, 2002–2012

(92) Rodger, A., Norden, B. *Circular Dichroism and Linear Dichroism*. Oxford University Press, Oxford, New York, Tokyo. 1997.

(93) Rodger, A., Marington, R., Geeves, M. A., Hicks, M., de Alwis, L., Halsall, D. J., Dafforn, T. R. (2006) Looking at long molecules in solution: what happens when they are subjected to Couette flow? *Phys. Chem. Chem. Phys. 8*, 3161–3171.

(94) Wirth, M., Buchardt, O., Koch, T., Nielsen, P. E., Norden, B. (1988) Interactions between DNA and mono(aminoacridines), bis(aminoacridines), tris(aminoacridines), tetrakis(aminoacridines), and hexakis(aminoacridines) - a linear and circular-dichroism, electric orientation relaxation, viscometry, and equilibrium study. *J. Am. Chem. Soc. 110*, 932–939.

(95) Satyanarayana, S., Dabrowiak, J. C., Chaires, J. B. (1992) Neither D nor L-tris(phenanthroline)ruthenium(II) binds to DNA by classical intercalation. *Biochemistry 31*, 9319–9324.

(96) Barone, G., Gennaro, G., Giuliania, A. M., Giustini, M. (2016) Interaction of Cd(II) and Ni(II) terpyridine complexes with model polynucleotides: a multidisciplinary approach. *RSC Adv. 6*, 4936–4945.

(97) Baruah, H., Barry, C. G., Bierbach, U. (2004) Platinum-intercalator conjugates: from DNA targeted cisplatin derivatives to adenine binding complexes as potential modulators of gene regulation. *Curr. Top. Med. Chem. 4*, 1537–1549.

(98) Coleman, L. W., Rohr, L. R., Bronstein, I. B., Holden, J. A. (2002) Human DNA topoisomerase I: An anticancer drug target present in human sarcomas. *Human Pathol. 33*, 599–607.

(99) Palumbo, M., Gatto, B., Moro, S., Sissi, C., Zagotto, G. (2002) Sequence-specific interactions of drugs interfering with the topoisomerase-DNA cleavage complex. *Biochim. Biophys. Acta 1587*, 145–154.

(100) Ulukan, H., Swaan, P. W. (2002) Camptothecins - A review of their chemotherapeutic potential. *Drugs 62*, 2039–2057.

(101) Malina, J., Vrana, O., Brabec, V. (2009) Mechanistic studies of the modulation of cleavage activity of topoisomerase I by DNA adducts of mono- and bi-functional Pt^{II} complexes, *Nucleic Acids Res. 37*, 5432-5442.

(102) Webb, M. R., Ebeler, S. E. (2003) A gel electrophoresis assay for the simultaneous determination of topoisomerase I inhibition and DNA intercalation. *Anal. Biochem*. 321, 22–30.

(103) Peixoto, P., Bailly, C., David-Cordonnier, M.-H. In Fox, R. K. (ed.), Drug-DNA Interaction Protocols. Humana Press, Totowa, N. J, 2010, pp. 235–256.

(104) Malina, J., Farrell, N.P., Brabec, V. (2014) Substitution-inert trinuclear platinum complexes efficiently condense/aggregate nucleic acids and inhibit enzymatic activity. *Angew. Chem. Int. Ed. Engl*. 53, 12812-12816.

(105) Janočková, J., Plšíková, J., Koval' J., Jendželovský R., Mikeš, J., Kašpárková, J, Brabec, V, Hamuľaková, S.,Fedoročko, P., Kožurková, M. (2015) Tacrine derivatives as dual topoisomerase I and II catalytic inhibitors. *Bioorg. Chem. 59*, 168-176.

(106) Khoo, C. P., Micklem, K., Watt, S. M. (2011) A comparison of methods for quantifying angiogenesis in the Matrigel assay in vitro. *Tissue Eng. Part C, Methods 17*, 895–906.

(107) Hu, J., Verkman, A. S. (2006) Increased migration and metastatic potential of tumor cells expressing aquaporin water channels. *FASEB J. 20*, 1892–1894.

(108) Usón, R., Laguna, A., Laguna, M., Briggs, D. A., Murray, H. H., Fackler, J. P. (1989) (Tetrahydrothiophene)gold(I) or gold(III) complexes. *Inorg. Synth. 26*, 85–91.

(109) Brabec, V., Palecek, E. (1976) Interaction of nucleic-acids with electrically charged surfaces. II. Conformational changes in double-helical polynucleotides. *Biophys. Chem. 4*, 79–92.

(110) Brabec, V., Palecek, E. (1970) The influence of salts and pH on polarographic currents produced by denatured DNA. *Biophysik 6*, 290–300.

(111) Sheldrick, G. M. *SHELX-97*, An integrated system for solving and refining crystal structures from diffraction data; University of Göttingen: Göttingen Germany, 1997.

(112) Chen, T. R. (1975) Microscopic demonstration of mycoplasma contamination in cell cultures and cell culture media. *TCA Manual 1*, 229–232.

(113) Novohradsky, V., Zerzankova, L., Stepankova, J., Vrana, O., Raveendran, R., Gibson, D., Kasparkova, J., Brabec, V. (2015) New insights into the molecular and epigenetic effects of antitumor Pt(IV)-valproic acid conjugates in human ovarian cancer cells. *Biochem Pharmacol. 95*, 133-144.

(114) Wachter, E., Howerton, B. S., Hall, E. C., Parkin, S., Glazer, E. C. (2014) A new type of DNA "light-switch": a dual photochemical sensor and metalating agent for duplex and G-quadruplex DNA. *Chem. Commun. 50*, 311–313.

(115) Kostrhunova, H., Malina, J., Pickard, A.J., Stepankova, J., Vojtiskova, M., Kasparkova, J., Muchova, T., Rohlfing, M. L., Bierbach, U., Brabec, V. (2011) Replacement of a thiourea with an amidine group in a monofunctional platinum-acridine antitumor agent. Effect on DNA interactions, DNA adduct recognition and repair. *Mol. Pharm. 8,* 1941-1954.

(116) Wachter, E., Moyá, D., Parkin, S., Glazer, E. C. (2016) Ruthenium Complex "Light Switches" that are Selective for Different G-Quadruplex Structures. *Chemistry 22*, 550-559.

1
2
3
4
5
6
7
8
9
10
11
12
13
14
15
16
17
18
19
20
21
22
23
24
25
26
27
28
29
30
31
32
33
34
35
36
37
38
39
40
41
42
43
44
45
46
47
48
49
50
51
52
53
54
55
56
57
58
59
60

✓ Highly cytotoxic drugs
✓ Vasculogenic mimicry inhibitors
✓ Caspase-3 activation
✓ Topo I inhibitors

λ_{ex} = 590 and 488 nm

2
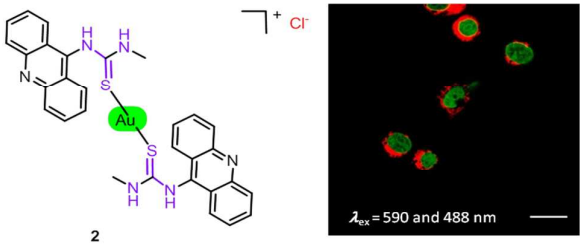
For Table of Contents Only (TOC)

47